© 2021. Published by The Company of Biologists Ltd | Development (2021) 148, dev189258. doi:10.1242/dev.189258

RESEARCH ARTICLE

Extensive crosstalk of G protein-coupled receptors with the Hedgehog signalling pathway

Farah Saad[1,2] and David R. Hipfner[1,2,3,*]

ABSTRACT

Hedgehog (Hh) ligands orchestrate tissue patterning and growth by acting as morphogens, dictating different cellular responses depending on ligand concentration. Cellular sensitivity to Hh ligands is influenced by heterotrimeric G protein activity, which controls production of the second messenger 3′,5′-cyclic adenosine monophosphate (cAMP). cAMP in turn activates Protein kinase A (PKA), which functions as an inhibitor and (uniquely in *Drosophila*) as an activator of Hh signalling. A few mammalian Gαi- and Gαs-coupled G protein-coupled receptors (GPCRs) have been shown to influence Sonic hedgehog (Shh) responses in this way. To determine whether this is a more-general phenomenon, we carried out an RNAi screen targeting GPCRs in *Drosophila*. RNAi-mediated depletion of more than 40% of GPCRs tested either decreased or increased Hh responsiveness in the developing *Drosophila* wing, closely matching the effects of Gαs and Gαi depletion, respectively. Genetic analysis indicated that the orphan GPCR Mthl5 lowers cAMP levels to attenuate Hh responsiveness. Our results identify Mthl5 as a new Hh signalling pathway modulator in *Drosophila* and suggest that many GPCRs may crosstalk with the Hh pathway in mammals.

KEY WORDS: Hedgehog signalling, G protein-coupled receptor (GPCR), Heterotrimeric G protein, Cyclic AMP (cAMP), *Drosophila*

INTRODUCTION

The Hedgehog (Hh) signalling pathway is crucial for patterning of embryonic tissues (Briscoe and Thérond, 2013; Jiang and Hui, 2008). Hh ligands such as Sonic hedgehog (Shh) in vertebrates and Hh in *Drosophila* are morphogens, diffusing through tissues from localized sources and eliciting differential transcriptional responses in distant cells, dependent on ligand concentration and time of exposure (Briscoe and Small, 2015; Jiang and Hui, 2008). Some high-threshold Hh target genes, such as *Nkx2.2* in the mouse neural tube or *patched* (*ptc*) in the *Drosophila* wing imaginal disc, are expressed only close to the source of Hh, where concentration is high and cells have been exposed for the longest time. In contrast, low-threshold targets, such as *decapentaplegic* (*dpp*) in flies, are expressed where ligand levels are lower (Placzek and Briscoe, 2018; Strigini and Cohen, 1997).

Hh concentration gradients are translated into activity of the cubitus interruptus (Ci) and Glioma-associated oncogene (GLI) family transcription factors in vertebrates and flies, respectively, through a conserved signalling pathway (Briscoe and Thérond, 2013; Hui and Angers, 2011). In the absence of Hh, activity of the atypical G protein-coupled receptor (GPCR) Smoothened (Smo) is suppressed by the Hh receptor Ptc (Denef et al., 2000). In this state, Ci/GLI proteins undergo partial proteolysis to truncated proteins (CiR/GLIR) that repress transcription of some target genes (Aza-Blanc et al., 1997; Méthot and Basler, 1999; Niewiadomski et al., 2014; Price and Kalderon, 1999; Wang et al., 2000). Hh binding to Ptc relieves its inhibition of Smo (Denef et al., 2000; Ingham et al., 2000), which undergoes extensive phosphorylation and adopts an active conformation (Apionishev et al., 2005; Chen et al., 2011; Jia et al., 2004; Zhang et al., 2004; Zhao et al., 2007). Smo signals through a conserved pathway to block CiR/GLIR formation and alleviate inhibition of full-length Ci/GLI proteins at multiple levels, enabling them to transcriptionally activate their targets (Briscoe and Thérond, 2013; Hui and Angers, 2011). The levels of *Drosophila* Smo phosphorylation and activity are correlated with Hh levels (Fan et al., 2012; Su et al., 2011), suggesting that Hh ligand concentration gradients are converted to intracellular signalling gradients that can explain, in part, the differential activation of low- and high-threshold target genes.

Recently, a unique mechanism for shaping Hh responses involving the second messenger 3′,5′-cyclic adenosine monophosphate (cAMP) was identified. In both flies and mammals, the level of cAMP in cells helps determine their sensitivity to Hh ligands (Praktiknjo et al., 2018; Pusapati et al., 2018). cAMP is produced from ATP by adenylyl cyclases whose activity is controlled by GPCRs signalling through heterotrimeric G proteins to stimulate (Gαs) or inhibit (Gαi, Gαo) cAMP synthesis (Wettschureck and Offermanns, 2005). In mammalian cells, activity of the GPCR Gpr161 stimulates cAMP production through Gαs (Mukhopadhyay et al., 2013). Mutation of Gpr161 decreases the amount of Shh needed for transcriptional activation of target genes and expands the distance over which medium- and high-threshold target genes are activated by Shh in the mouse neural tube (Mukhopadhyay et al., 2013; Pusapati et al., 2018), suggesting that cAMP desensitizes mammalian cells to Shh. This is consistent with reports that Gαs and the Gαs-coupled GPCRs PAC1 and Gpr17 suppress Shh target gene expression in mammalian cells (Cohen et al., 2010; He et al., 2014; Iglesias-Bartolome et al., 2015; Niewiadomski et al., 2013; Rao et al., 2016; Yatsuzuka et al., 2019), whereas Gαi and the Gαi-coupled GPCRs Cxcr4 and Gpr175 enhance their expression (Klein et al., 2001; Riobo et al., 2006; Singh et al., 2015). A similar mechanism appears to exist in *Drosophila*, where depletion of Gαi or Gαs increased or decreased, respectively, the range over which expression of some Hh target genes is activated in the developing wing (Praktiknjo et al., 2018). The effects of Gα depletion suggest that cAMP increases Hh sensitivity in *Drosophila* rather than decreasing it, consistent with effects observed when directly activating Gαi or Gαs in discs

[1]Institut de recherches cliniques de Montréal, 110 Pine Avenue West, Montreal H2W 1R7, QC, Canada. [2]Department of Biology, McGill University, Montreal H3A 1B1, QC, Canada. [3]Département de médecine, Université de Montréal, Montreal H3C 3J7, QC, Canada.

*Author for correspondence (david.hipfner@ircm.qc.ca)

D.R.H., 0000-0002-2265-5871

Handling Editor: Thomas Lecuit
Received 7 February 2020; Accepted 19 February 2021

Development (2021) 148, dev189258. doi:10.1242/dev.189258

(Cheng et al., 2012). There is also evidence that cAMP can inhibit Hh target gene expression in flies (Ogden et al., 2008).

These effects of cAMP are likely due to changes in the activity of Protein kinase A (PKA), the main cellular target of cAMP. In flies and mammals, PKA phosphorylates and inhibits Ci/GLI proteins (Niewiadomski et al., 2014; Price and Kalderon, 1999; Wang et al., 1999) by a conserved mechanism (Marks and Kalderon, 2011), likely explaining the inhibitory effect of cAMP on Hh target gene expression in flies (Ogden et al., 2008). PKA also plays a unique positive role in the *Drosophila* Hh pathway, where it is the principal kinase responsible for phosphorylating Smo to activate signalling (Apionishev et al., 2005; Jia et al., 2004; Zhang et al., 2004). In fact, moderate overexpression of the PKA catalytic subunit hyperactivates *Drosophila* Smo and is sufficient to expand the domain over which Hh target genes are expressed (Jia et al., 2004).

Regulation of cAMP production in Hh-stimulated cells may be direct. Mammalian Smo can couple to Gαi (Qi et al., 2019; Riobo et al., 2006; Shen et al., 2013), and *Drosophila* Smo can activate $G\alpha_i$ and $G\alpha_s$ (Ogden et al., 2008; Praktiknjo et al., 2018). However, it is clear that other GPCRs are involved. A few have been identified in mammals, but it is not known whether these represent the exception or whether many GPCRs among the hundreds encoded in mammalian genomes have this capacity.

Drosophila represents a simpler system for studying GPCRs, with just 116 GPCRs encoded in the genome. These receptors have traditionally been classified into four families – the Rhodopsin-like Class A, Secretin-like Class B, Glutamate Class C and Atypical or Frizzled-like Class F (Table S1) – although more recent phylogenetic analyses reveal a more nuanced organization (Hanlon and Andrew, 2015). We assessed the extent of GPCR crosstalk with the Hh pathway by screening for GPCRs expressed in the *Drosophila* wing imaginal disc that influence Hh responses. We found that RNA interference (RNAi)-mediated depletion of more than 40% of GPCRs tested phenocopied either Gαs or Gαi depletion, diminishing or enhancing sensitivity to Hh, respectively. More in-depth analysis of one of these GPCRs, Mthl5, suggests that it attenuates Hh signalling by lowering the level of cAMP in cells. These results indicate that GPCR crosstalk with the Hh pathway in mammals is likely to be extensive rather than limited to just a few receptors.

RESULTS

Identification of GPCRs producing Gαs- or Gαi-like depletion phenotypes in the wing

Hh signalling controls the growth of the *Drosophila* wing along the anterior-posterior (A-P) axis and directly patterns the central region of the wing between longitudinal veins L3 and L4 (highlighted in Fig. 1A). We have previously shown that this depends on the activity of Gαs and Gαi, as depletion of either leads to a spectrum of defects associated with changes in Hh target gene expression (Praktiknjo et al., 2018). Wings in which Gαs was depleted by expressing a short RNA hairpin (using the *nubbin*-GAL4 driver) were smaller and not properly inflated (Fig. 1B) (Praktiknjo et al., 2018), a process known to require Gαs activation by the GPCR Rickets (Rk) (Baker and Truman, 2002; Kimura et al., 2004). Gαi-depleted wings showed an ectopic vein phenotype similar to that caused by *dpp* overexpression in the developing wing pouch (De Celis, 1998) and an increase in the area of the region bounded by wing veins L3 and L4 relative to total wing area (Fig. 1C, quantified in Fig. 1S) (Praktiknjo et al., 2018). This is a phenotype specifically associated with increased Hh signalling (Mullor et al., 1997).

These phenotypes suggested that some GPCRs are actively signalling through Gαs and Gαi in wing discs, and that their activity affects cell responses to Hh. We reasoned that reducing the levels of such GPCRs would produce a similar spectrum of phenotypes, depending on the Gα subunit to which they couple. To investigate this, we first carried out RNAseq analysis to identify which GPCRs are expressed in late third instar wing discs. We detected substantial expression of roughly one-quarter of the 116 GPCR-encoding genes, and at least some expression of more than half (Fig. 1D). To simplify our analysis, we excluded *smo* and the various *frizzled* homologues belonging to the atypical class F of the GPCR family (Hanlon and Andrew, 2015). We focused on 22 of the most highly expressed remaining GPCRs, most from the more classical Class A/B/C receptors (Table 1).

We expressed dsRNA transgenes targeting each of these GPCRs throughout the developing wing pouch and examined the effects on the adult wing. We observed a range of phenotypes upon depletion of 15 of the 22 GPCRs with at least one RNAi strain (Table S2). At the most extreme, depletion of the class A receptors Trapped in endoderm 1 (Tre1) or CCK-like receptor at 17D3 (CCKLR-17D3), or of the class C receptor CG32447 was lethal, with rare wingless escapers in the case of CCKLR-17D3 and CG32447.

Seven GPCRs produced depletion phenotypes more similar to Gαs. These included three Secretin-like class B adhesion GPCRs [the Methusaleh (Mth)-like family receptors Mthl6, Mthl8 and Mthl9], which caused a severe wing inflation defect (Fig. 1E-G), and four others (Rk, Mthl4, Stan and CG15744) that gave rise to uneven wings consistent with weaker inflation defects (Fig. 1H-L) and to a decrease in wing size (Fig. 1M). As mentioned above, Rk is known to stimulate cAMP production through Gαs.

On the other hand, depletion of four GPCRs (Mth, Mthl5, GABA-B-R2 and Cirl) caused Hh gain-of-function phenotypes similar to those observed upon Gαi depletion (Fig. 1N-R). Most notably, depletion of Mth, Mthl5 and GABA-B-R2 caused the appearance of extensive ectopic veins, and the ratio of L3-L4 to total wing area was significantly increased in all four cases (Fig. 1S). Interestingly, three of these GPCRs (or their orthologues) – GABA-B-R2, Mthl5 and Cirl – have been shown to couple to inhibitory Gα proteins to lower cellular cAMP levels (Franek et al., 1999; Patel et al., 2016; Scholz et al., 2017).

Depletion of some GPCRs impairs Hh target gene expression

To confirm that these wing phenotypes were due to altered Hh signalling, we analysed Hh target gene expression earlier in imaginal discs. Hh is expressed by cells of the posterior compartment and diffuses into the anterior compartment to form a concentration gradient that stabilizes full-length Ci (Ci^{155}) in a central stripe of responding anterior cells, where it activates target gene expression (Fig. 2A). The low threshold target gene *dpp* is expressed in a broad stripe of cells, and the higher-threshold target *ptc* is expressed over a narrower domain. Quantification of fluorescence intensities along the A-P axis indicated that the domains of Ci stabilization and *dpp* and *ptc* expression are of roughly equal width in dorsal and ventral compartments (Fig. 2B). As we previously showed (Praktiknjo et al., 2018), Gαs depletion in the dorsal compartment of the wing disc (using the *ap*-GAL4 driver) dampened responsiveness to low levels of Hh. This was characterized by a narrowing of the range over which *dpp* was expressed in the dorsal compartment compared with the wild-type ventral compartment, with little effect on Ci stabilization or *ptc* expression (Fig. 2C,D).

To look at the effects of GPCR depletion, we started with the seven GPCRs whose depletion caused inflation defects. Of these, six had effects on *dpp* expression that phenocopied Gαs depletion. Depletion of Mthl4 (Fig. 2E,F), Mthl8 (Fig. 2G,H), Mthl9 (Fig. 2I,J),

Development (2021) 148, dev189258. doi:10.1242/dev.189258

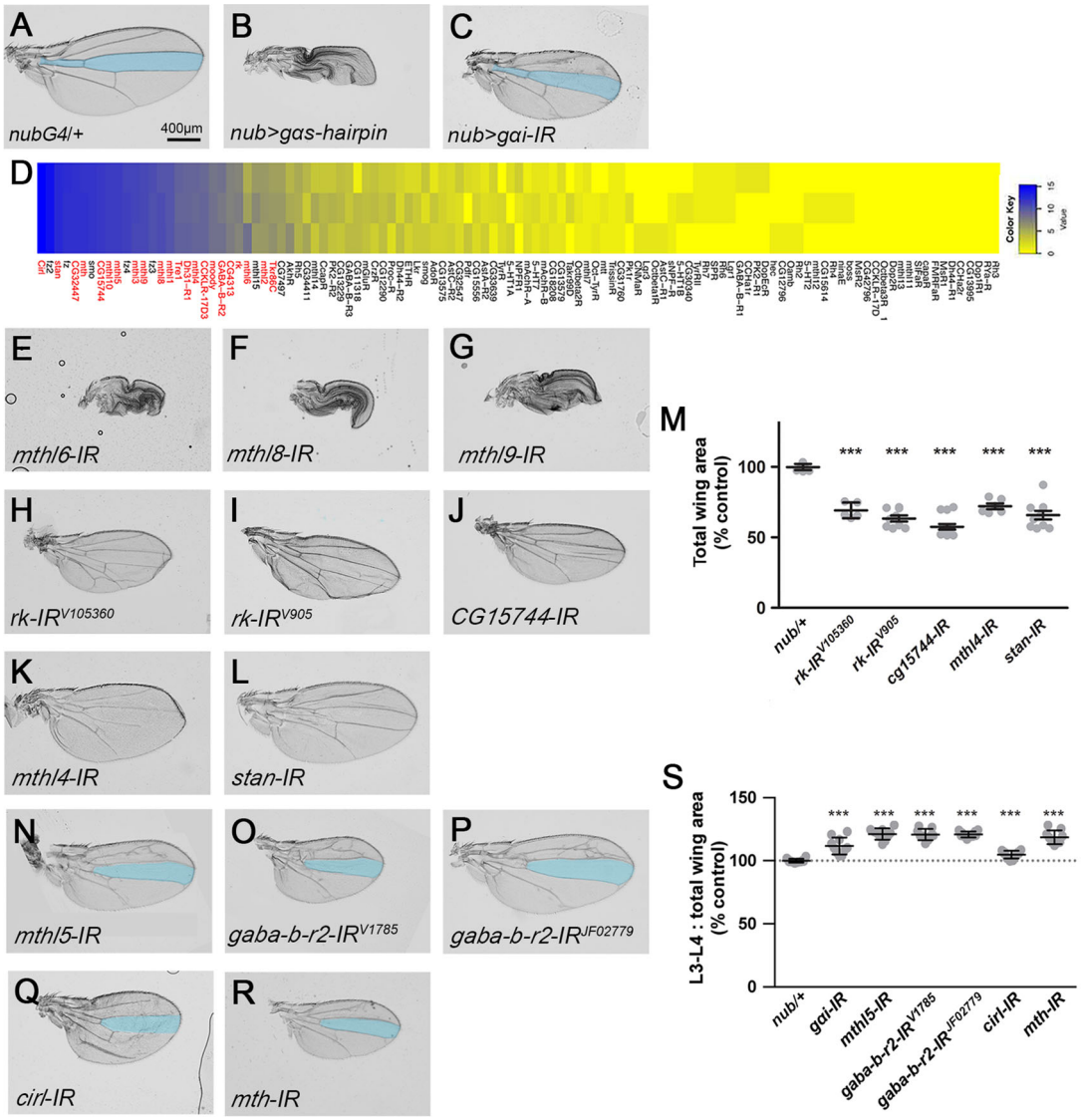

Fig. 1. Adult wing phenotypes arising from RNAi depletion of GPCRs expressed in the wing disc. (A) *nub*-GAL4/+ adult *Drosophila* wing showing wild-type patterning. L3-L4 region is shaded blue. (B) Wing from a fly expressing a short hairpin targeting *gαs* under the control of *nub*-GAL4. (C) Wing from a fly expressing a long dsRNA targeting *gαi* under the control of *nub*-GAL4. (D) Heat map showing the RNA expression levels in late third instar wing discs of the 116 GPCRs encoded in the *Drosophila* genome. GPCRs included in the RNAi screen are indicated in red. (E-S) Wings from flies expressing dsRNAs targeting the indicated GPCR transcripts throughout the developing wing pouch (E-L,N-R). Phenotypes resembling Gαs depletion include severe (E-G) or weak (H-L) inflation defects and a decrease in wing size (H-L, quantified in M). Phenotypes resembling Gαi depletion include ectopic veins and an increased L3-L4:total wing area ratio (N-R, quantified in S), typical of Hh gain of function. All wing images are shown at the same magnification (indicated in A). Data are mean±s.d. ***P<0.0001 (unpaired two-tailed t-test). Comparable results were obtained in two experiments.

Rk (Fig. 2K,L), CG15744 (Fig. 2M,N) or Stan (Fig. 2O,P) decreased the range of *dpp* expression to varying degrees. The sole exception was Mthl6, the depletion of which had no effect (data not shown).

We also assessed the effects of depleting selected GPCRs on expression of the high-threshold Hh target gene *engrailed* (*en*). *en* is expressed throughout the posterior compartment in a Hh-independent manner, but in late third instar is upregulated in the first few rows of anterior boundary cells in response to high levels of Hh (Fig. S1), where it is thought to lower *dpp* expression (Raftery et al., 1991; Strigini and Cohen, 1997). En protein levels were roughly symmetrical between the dorsal and ventral compartments (Fig. S1A,B). Gαs-depleted Hh-responding cells activated *en* expression, although protein levels were somewhat (~20%) lower than normal (Fig. S1C,D). Rk depletion had a similar effect (Fig. S1E,F). However, in both cases it was difficult to attribute this to a specific defect in Hh signalling, as Hh-independent posterior compartment En levels were, unexpectedly, also lower in dsRNA-expressing cells.

Depletion of some GPCRs enhances Hh target gene expression

Depleting Gαi had the opposite effect of Gαs depletion. As we have shown previously (Praktiknjo et al., 2018), Gαi-depleted discs showed a Hh gain-of-function phenotype characterized by an increase in the range over which Ci stabilization and *dpp* (and to a lesser extent, *ptc*) expression were detected (Fig. 3A,B). Among the four GPCRs whose depletion caused Hh gain-of-function-like phenotypes, all [Mthl5 (Fig. 3C,D), GABA-B-R2 (Fig. 3E,F), Mth (Fig. 3G,H) and Cirl (Fig. 3I,J)] significantly increased the level and/or range of *dpp* expression when depleted, phenocopying Gαi

Development (2021) 148, dev189258. doi:10.1242/dev.189258

Table 1. GPCRs tested in the adult wing screen

Name	CG number	GPCR family (as per Hanlon and Andrew, 2015)	G-protein coupling
Moody	CG4322	Rhodopsin (class A)	Gαi/o (Schwabe et al., 2005)
Trapped in endoderm 1 (Tre1)	CG3171	Rhodopsin (class A)	Gαo (Yoshiura et al., 2012)
CG4313	CG4313	Rhodopsin (class A)	Not characterized
Rickets (Rk)	CG8930	Rhodopsin (class A, Glycoprotein subfamily)	Gαs (Kimura et al., 2004)
Cholecystokinin-like receptor at 17D3 (CCKLR-17D3)	CG32540	Rhodopsin (class A, Peptide A subfamily)	Gαs (Chen and Ganetzky, 2012)
Tachykinin-like receptor at 86C (Tkr86C)	CG6515	Rhodopsin (class A, Peptide A subfamily)	Not characterized
Diuretic hormone 31 receptor 1 (Dh31-R1)	CG32843	Secretin-like (Class B, Secretin subfamily)	Not characterized
Methuselah (Mth)	CG6936	Secretin (Class B, Methuselah subfamily)	Not characterized
Methuselah-like 1 (Mthl1)	CG4521	Secretin (Class B, Methuselah subfamily)	Not characterized
Methuselah-like 2 (Mthl2)	CG17795	Secretin (Class B, Methuselah subfamily)	Not characterized
Methuselah-like 3 (Mthl3)	CG6530	Secretin (Class B, Methuselah subfamily)	Not characterized
Methuselah-like 4 (Mthl4)	CG6536	Secretin (Class B, Methuselah subfamily)	Not characterized
Methuselah-like 5 (Mthl5)	CG6965	Secretin (Class B, Methuselah subfamily)	Gαo (Patel et al., 2016)
Methuselah-like 6 (Mthl6)	CG16992	Secretin (Class B, Methuselah subfamily)	Not characterized
Methuselah-like 8 (Mthl7)	CG32475	Secretin (Class B, Methuselah subfamily)	Not characterized
Methuselah-like 9 (Mthl8)	CG17084	Secretin (Class B, Methuselah subfamily)	Not characterized
Methuselah-like 10 (Mthl10)	CG17061	Secretin (Class B, Methuselah subfamily)	Not characterized
Metabotropic GABA-B receptor subtype 2 (GABA-B-R2)	CG6706	Metabotropic glutamate receptors (Class C)	Gαi (Wojcik and Neff, 1984)
Starry night (Stan)	CG11895	Frizzled (Class F, Atypical subfamily)	Not characterized
Calcium-independent receptor for α-latrotoxin (Cirl)	CG8639	Frizzled (Class F, Atypical subfamily)	Gαi (Scholz et al., 2017)
CG32447	CG32447	Not classified	Not characterized
CG15744	CG15744	Not classified	Not characterized

depletion. The maximum level of *ptc* expression or the width of its expression domain were also significantly increased, and all but Cirl (which had the weakest adult phenotype) significantly increased the range and level of Ci stabilization.

Depletion of Gαi, Mthl5 or Cirl all had similar effects on En. Anterior *en* was still activated in each case, but protein levels were lower (Fig. S1G-L). As with Gαs depletion, Hh-independent levels of En in the posterior compartment were also lower, confounding interpretation of the results. We noted that DAPI staining intensity was also noticeably lower in the dorsal compartment, consistent with reduced cellularity due to an elevated level of apoptosis in the depleted cells (see below and data not shown). When corrected for this decrease, En levels in these backgrounds were similar to those observed in Gαs- and Rk-depleted discs, despite the opposite effects of Gαs and Rk on *dpp* expression. This suggests that changes in *en* expression alone are unlikely to explain the expansion of *dpp* expression in Gαi/Mthl5/Cirl-depleted discs.

Taken together, our screen results indicate that 45% (10 of 22) of the expressed GPCRs that we tested are capable of crosstalking with the Hh pathway as part of their normal function. The similarity between GPCR and G-protein depletion phenotypes suggests that they do so by signalling through either Gαi or Gαs, as some GPCRs do in mammals.

Mthl5 is expressed throughout the wing disc and is required for normal development

We chose one little-characterized GPCR candidate for further testing. Mthl5 is an orphan GPCR belonging to the Mth-like GPCR family. This evolutionarily ancient family of proteins shows close resemblance to the Secretin family GPCRs, descended from the larger family of adhesion GPCRs (Langenhan et al., 2013; Patel et al., 2012). Mthl5 does not have a clear orthologue in mammals.

mthl5 is expressed at high levels in the developing *Drosophila* embryonic heart where it is required for normal morphogenesis of the aorta (Patel et al., 2016). To assess where *mthl5* is expressed in discs, we generated an antiserum against the large extracellular N-terminal domain of the protein. Immunostaining with this antiserum revealed a ubiquitous distribution of the protein in wing discs (Fig. 4A), with Mthl5 protein accumulating preferentially in the apical region of cells (Fig. 4B). Mthl5 immunostaining was much reduced in *mthl5*-depleted disc cells (Fig. S2), confirming that the antiserum is specific and that the *mthl5* dsRNA transgene is functional.

The *mthl5* gene is situated on chromosome 3R in the intron of another gene (*CG31368*), transcribed in the opposite orientation (Fig. 4C). There are two isoforms (*mthl5-RA* and *mthl5-RB*) that differ by just three nucleotides (and one amino acid) due to alternate use of neighbouring splice sites in exon 2. The Gene Disruption Project generated a fly strain bearing a Minos element inserted in the coding region of *mthl5* (Mi{ET1}CG31368^{MB03076}, which we re-designate *mthl5*^{MB03076}). The insertion in this strain is in exon 5, which is common to both *mthl5* isoforms (Fig. 4C), a finding we confirmed by sequencing of genomic PCR products from the insertion flanks. *In silico* predictions showed that the *mthl5*^{MB03076} mutation introduces a stop codon within predicted transmembrane domain 5 of the 7-transmembrane core of the protein, potentially leaving the long extracellular N terminus intact but deleting the short cytoplasmic C-terminal tail.

Less than one-third of *mthl5*^{MB03076} homozygous mutants (55/176 expected) survived to adulthood. The majority died at third instar or pupal stages. Survival was also low (47/101 expected) for trans-heterozygotes of *mthl5*^{MB03076} and *Df(3R)BSC514*, a chromosomal deficiency uncovering the *mthl5* gene. Several defects were apparent in *mthl5* mutant wing discs. Both *mthl5*^{MB03076} and *mthl5*^{MB03076}/*Df(3R)BSC514* mutant discs were on average about 30-50% larger than wild-type controls (Fig. 4D-G). The overgrowth was most noticeable in the pleura and hinge regions surrounding the pouch. In fact, the A-P length of the wing pouch in *mthl5*^{MB03076} mutant discs was similar to wild type (Fig. 4H). Other morphological defects were frequently observed, including a cleft along the A-P boundary of the wing pouch in many *mthl5*^{MB03076} mutant discs (arrow in Fig. 4E). Pyknotic nuclei were present on the basal side of the wing pouch, and activated Caspase 3 immunostaining indicated that apoptosis levels were high (Fig. 4I,J). We conclude that Mthl5 plays an important role in regulating growth and cell survival during wing disc development.

Development (2021) 148, dev189258. doi:10.1242/dev.189258

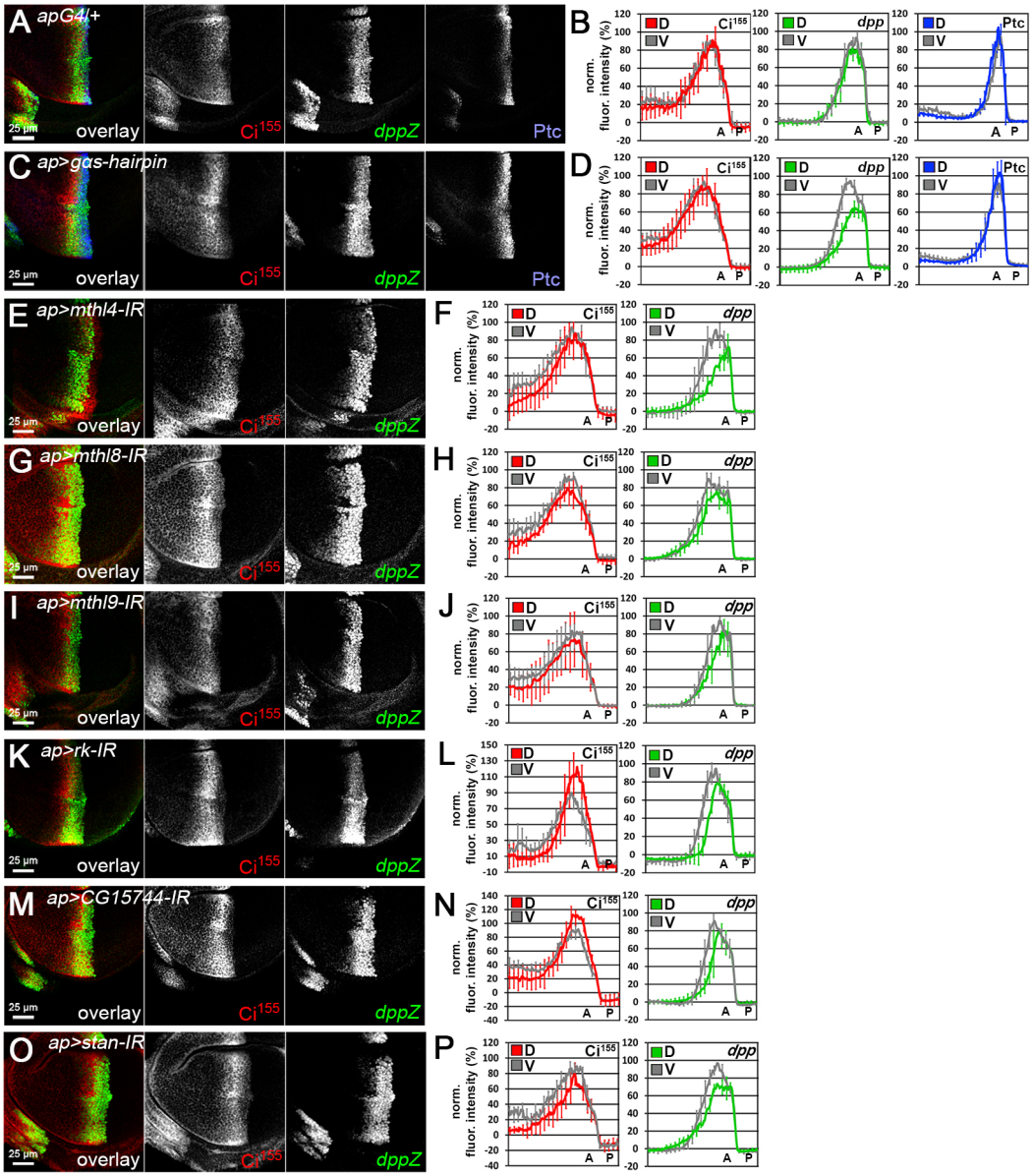

Fig. 2. Depletion of six GPCRs lowers Hh responsiveness in discs. (A,B) Confocal image of an *ap*-GAL4/+ wing imaginal disc (A) immunostained using antibodies against Ci^{155} (red), β-Gal (expressed from a *dpp* enhancer trap; green) and Ptc (blue) to show the wild-type expression pattern. In these and all subsequent images, discs are oriented with the dorsal compartment toward the top and the posterior compartment toward the right. Fluorescence intensity along the A-P axis in dorsal (D) versus ventral (V) compartments is quantified in B. (C,D) Wing disc expressing a short hairpin targeting *gαs* under *ap*-GAL4 control (C), immunostained as in A. Fluorescence intensity is quantified in D. (E-P) Wing discs expressing dsRNAs targeting the indicated GPCR under *ap*-GAL4 control (E,G,I,K,M,O) immunostained using antibodies against Ci^{155} (red) and β-Gal (expressed from a *dpp* enhancer trap; green). Fluorescence intensities are quantified in F, H,J,L,N,P. Data are mean±s.d. for five wing discs. Error bars are indicated every 10th data point. Experiments were performed at least twice. Compared with 15 control discs (A), phenotypes were seen in 15/18 discs (C), 9/9 discs (E), 9/11 discs (G), 6/10 discs (I), 20/20 discs (K), 15/28 discs (M) and 15/24 discs (O).

Hh signalling is upregulated in mthl5 mutants

The pleural overgrowth and A-P boundary clefting in *mthl5* mutant discs are reminiscent of phenotypes caused by increased Hh activity (Umemori et al., 2007). To determine if Hh signalling is upregulated in the mutants, as it is when Mthl5 is depleted, we analysed the adult wing phenotypes of escaper flies. Compared with control (w^{1118}) or $mthl5^{MB03076}$ heterozygotes (Fig. 5A,B), the wings of $mthl5^{MB03076}$ homozygous flies were somewhat variable in appearance, ranging from roughly normal (Fig. 5C) to distorted with a proportionately larger anterior compartment (Fig. 5D). Total wing area was 20% smaller than controls (Fig. S3A), consistent with the elevated levels of apoptosis in mutant discs. The mean L3-L4:total wing area ratio was not significantly different from wild type (although 15 of 29 wings had a ratio higher than the highest value observed in wild-type wings), and was slightly increased relative to $mthl5^{MB03076}$ heterozygotes (Fig. 5H). However, the size of the anterior compartment relative to the posterior compartment (A:P ratio) was significantly greater in $mthl5^{MB03076}$ homozygotes (Fig. 5I). This resembles the low-level Hh gain-of-function phenotype caused by moderate overexpression of Smo throughout the wing pouch, which induces low level *dpp* expression throughout the anterior compartment (Maier et al., 2014) and anterior compartment overgrowth (Fig. 5E,I), but does not increase pathway activity sufficiently to broaden *ptc* expression (Maier et al., 2014) or

Development (2021) 148, dev189258. doi:10.1242/dev.189258

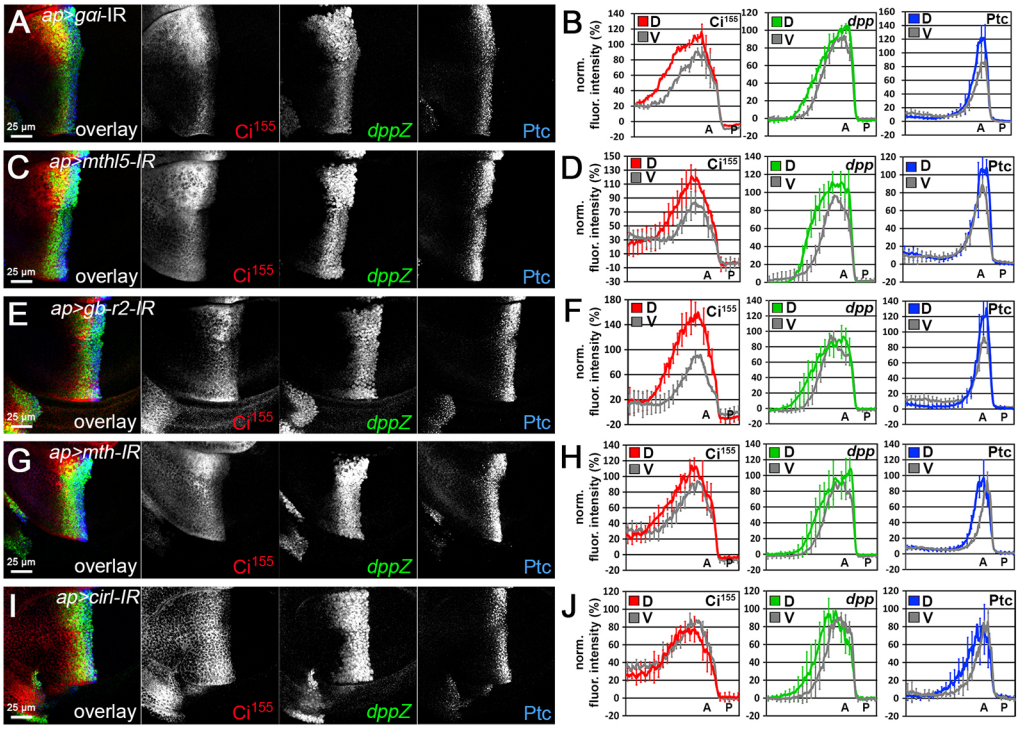

Fig. 3. Depletion of four GPCRs increases Hh responsiveness in discs. (A,B) Wing disc expressing dsRNA targeting *gαi* under *ap*-GAL4 control (A), immunostained using antibodies against Ci^{155} (red), β-Gal (expressed from a *dpp* enhancer trap; green) and Ptc (blue), and quantified in B. (C-J) Wing discs expressing dsRNAs targeting the indicated GPCR transcripts under *ap*-GAL4 control (C,E,G,I), immunostained as in A. Fluorescence intensities are quantified in D,F,H,J. Data are mean±s.d. of five wing discs. Error bars are indicated every 10 data points. Experiments were performed at least three times. Phenotypes were seen in 57/66 (*dpp*), 26/37 (Ci) and 19/27 (Ptc) discs examined (A); in 37/41 (*dpp*), 10/17 (Ci) and 13/17 (Ptc) discs (C); in 21/21 (*dpp*), 18/21 (Ci) and 9/9 (Ptc) discs (E); in 17/19 (*dpp*), 17/21 (Ci) and 15/21 (Ptc) discs (G); and in 21/23 (*dpp*), 1/11 (Ci) and 5/11 (Ptc) discs (I).

increase L3-L4 spacing (Fig. 5H). The phenotype of *mthl5*^{MB03076}/*Df(3R)BSC514* wings was more severe. Wings were smaller than controls (Fig. S3A). Although, again, somewhat variable in appearance (Fig. 5F,G), the L3:L4 area was consistently and significantly larger, and the relative overgrowth of the anterior compartment was more extreme (Fig. 5H,I). The stronger phenotype in *mthl5*^{MB03076}/*Df(3R)BSC514* animals suggests that *mthl5*^{MB03076} is not a null allele.

To confirm that these changes are due to altered Hh signalling, we examined Hh target gene expression in *mthl5* mutants. As in adult wings, the *mthl5*^{MB03076} homozygous disc phenotype was variable. Nearly half of *mthl5*^{MB03076} discs (14 of 32) showed clear signs of an expanded Hh pathway response. This was most apparent for *dpp*, which was expressed over a significantly wider anterior domain than in wild-type discs (Fig. 5J-L). There was also a statistically significant expansion of the anterior-most limit of Ci stabilization (Fig. 5M). These phenotypes were more extreme in *mthl5*^{MB03076}/*Df(3R)BSC514* discs. Ci^{155} often filled the anterior pouch (five out of 11 discs) (Fig. 5N), and in most cases the *dpp* and Ptc expression domains were substantially expanded (nine out of 11 and 11 of 13 discs examined, respectively) (Fig. 5N-P). Supporting the conclusion that target gene expansion in the mutants is due to loss of Mthl5 function, expression of a weaker Mthl5-GFP transgene (Mthl5-GFP^{weak}) that had little effect in a wild-type background significantly reduced the width of the *dpp* expression domain in *mthl5* mutants (Fig. S3B-F).

dpp can be upregulated in apoptotic disc cells that are prevented from dying by inhibition of caspases, with dramatic effect on tissue growth (Perez-Garijo et al., 2004; Ryoo et al., 2004). However, without caspase inhibition, Dpp does not appear to play a substantial role in increasing proliferation and tissue growth in these conditions (Perez-Garijo et al., 2009). Nonetheless, we examined whether ectopic *dpp* expression in *mthl5* mutant discs could be linked to high levels of apoptosis. *dpp*-LacZ expression was mainly restricted to anterior cells within the Hh-responding region, as normal, in *mthl5*^{MB03076} discs (Fig. 5Q) where apoptosis levels are high, and in *mthl5*-depleted discs where apoptosis was much lower (Fig. S4A,B). In both cases, expression was detected in some basal pyknotic nuclei, the vast majority of which were located below the endogenous *dpp* expression domain. This suggests that they arose from the death of normal *dpp*-expressing cells rather than from induction of *dpp* expression in dying cells. Next, we tested whether blocking apoptosis by dorsal compartment expression of P35 could prevent the expansion of *dpp* expression in *mthl5*^{MB03076}/*Df(3R)BSC514* mutants. Most of these discs were overgrown and disorganized, as seen in other contexts when widespread apoptosis is blocked (Martin et al., 2009). In the few discs that were interpretable, we observed Ci stabilization in a broad stripe of anterior cells up to three times the normal width (Fig. S4C). *dpp* expression was similarly expanded and mostly restricted to Ci^{155}-positive anterior compartment cells, indicative of ongoing and widespread Hh pathway activity. Together these results suggest that Hh signalling and not apoptosis is the main driver of expanded *dpp* expression when GPCRs like Mthl5 are depleted or mutated.

Disc overgrowth in *mthl5* mutants is driven by anterior expansion of *dpp* expression

Growth of lateral regions of the wing disc such as the pleura is controlled in part by Dpp (Barrio and Milán, 2017). We were therefore interested to test whether the disc overgrowth phenotype in *mthl5* mutants was due to increased Dpp signalling resulting from the anterior expansion of its expression domain. To examine *dpp* activity, we analysed the expression pattern of one of its high-threshold target genes, *spalt-major* (*salm*, visualized with a *salm-LacZ* enhancer trap) (de Celis et al., 1996). *salm* is normally expressed in anterior cells in the *dpp* expression domain and in a roughly symmetrical pattern extending towards the anterior and posterior margins of the wing pouch (Fig. 6A). In *mthl5*^{MB03076} discs, the anterior compartment domain of *spalt* expression was significantly wider, whereas the posterior domain was unchanged (Fig. 6B,C). This is consistent with an anterior expansion of Dpp signalling activity. To test whether Dpp was driving disc

Development (2021) 148, dev189258. doi:10.1242/dev.189258

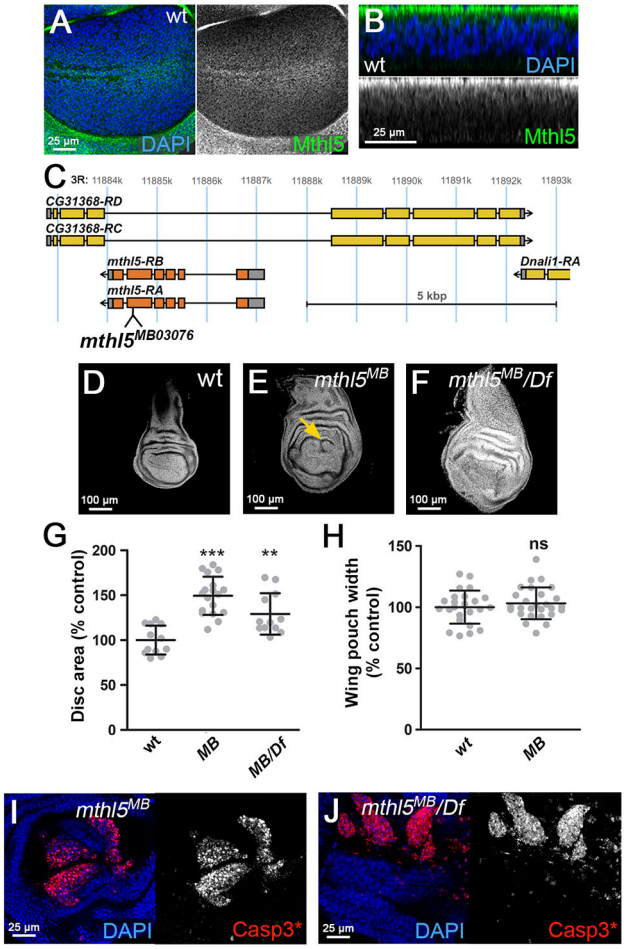

Fig. 4. Mthl5 is expressed in discs where it restricts disc growth and promotes cell survival. (A,B) Wild-type wing disc stained using anti-Mthl5 antiserum (green) and DAPI (blue). The images show discs in a single medial *xy* section (A) and in an orthogonal *xz* view (B). (C) Schematic of the *mthl5* locus, showing the location of the $mthl5^{MB03076}$ insertion in exon 5. (D-G) Wild-type (w^{1118}) (D), $mthl5^{MB03076}$ homozygous (E) or $mthl5^{MB03076}$/*Df(3R)BSC514* (F) wing discs stained with DAPI. $mthl5^{MB03076}$ discs often have a cleft at the A-P boundary (arrow in E) and are larger than normal [quantified in G; ***P*<0.01; ****P*<0.001 (unpaired two-tailed *t*-test)]. (H) Quantification of wing pouch width in wild-type and $mthl5^{MB03076}$ mutant discs. ns, *P*>0.05 (unpaired two-tailed *t*-test). (I,J) Confocal images of wing pouch region of discs from $mthl5^{MB03076}$ homozygous (I) and $mthl5^{MB03076}$/*Df(3R)BSC514* (J) larvae, immunostained for activated caspase 3 (red). Phenotype is seen in 12/12 (I) and 28/28 (J) discs.

overgrowth, we tried limiting Dpp pathway activity by lowering gene dose of *thick veins* (*tkv*), which encodes the Dpp receptor, using the tkv^{12} null allele. Unexpectedly, tkv^{12} heterozygous wing discs were larger than control w^{1118} discs (Fig. 6D,E,H). However, introduction of one copy of tkv^{12} significantly reduced the disc overgrowth phenotype of $mthl5^{MB03076}$ homozygotes, and improved wing disc morphology (Fig. 6F-H). These results suggest that anterior expansion of Hh pathway activity in the absence of Mthl5 indirectly drives disc overgrowth through a corresponding anterior expansion of Dpp signalling.

Mthl5 inhibits cAMP production and Hh target gene expression

The simplest explanation for the similarity between *mthl5* mutant and Gαi depletion phenotypes is that Mthl5 signals through Gαi to lower cAMP levels, decreasing sensitivity to Hh. Consistent with this, overexpression of a stronger-expressing Mthl5-GFP transgene caused a narrowing of the domain of *dpp* expression (Fig. 7A,B). We turned to *Drosophila* S2R+ cells to test this further. Transfection with an expression vector for Hh^{N}, a secreted and active form of the ligand, increased expression of the *ptc-Luciferase* (*ptc-Luc*) transcriptional reporter 13-fold compared with unstimulated cells (Fig. 7C). Co-expression of Mthl5-GFP significantly decreased Hh-induced *ptc-Luc* expression by almost 40% (Fig. 7C). Thus, in both flies and S2 cells, Mthl5 lowers Hh responsiveness.

To see whether Mthl5 affects cellular cAMP levels, we used the EPAC-BRET bioluminescence resonance energy transfer (BRET)-based cAMP biosensor, the BRET signal of which is inversely proportional to cAMP concentration (Cheng et al., 2012; Jiang et al., 2007). Compared with control cells, we observed a significant increase in net BRET signal (corresponding to a decrease in cAMP levels) in cells expressing Mthl5-GFP (Fig. 7D). Taken together, both loss- and gain-of-function results suggest that Mthl5 may normally limit Hh signalling by suppressing cAMP production.

Increased cAMP levels in *mthl5* mutants drive the expansion of Hh target gene expression

To examine this further, we tested whether manipulations that lower cAMP levels would rescue the *mthl5* mutant Hh target gene expression defect. We used two different approaches expected to specifically downregulate cAMP levels: expression of a mutant form of Gαi ($G\alpha i^{Q205L}$) that has a reduced 'off'-rate, causing it to signal longer when activated (Schaefer et al., 2001); and expression of Dunce (Dnc), a *Drosophila* phosphodiesterase that hydrolyses cAMP (Davis and Kiger, 1981). As we previously reported (Cheng et al., 2012), expression of $G\alpha i^{Q205L}$ did not alter Hh target gene expression in a wild-type background (Fig. 7E,F). However, in the $mthl5^{MB03076}$ background, $G\alpha i^{Q205L}$ significantly reduced the width of the *dpp* expression domain (Fig. 7G,H). Similarly, Dnc expression on its own only weakly reduced *dpp* expression (Fig. 7I,J), but had a stronger effect in $mthl5^{MB03076}$ mutants (Fig. 7K,L). These genetic interactions suggest that the increase in Hh signalling in *mthl5* mutants is due to an increase in cAMP levels.

As an independent confirmation, we tested the effect of limiting Pka activity on the *mthl5* mutant phenotype. Wing discs from larvae heterozygous for mutant alleles of *pka-C1* ($pka\text{-}C1^{76a3}$ and $pka\text{-}C1^{H2}$), encoding the Pka catalytic subunit were significantly larger than controls (Fig. 7M-O,S). However, when introduced into the $mthl5^{MB}$ background, both alleles significantly suppressed disc overgrowth (Fig. 7P-S), supporting the interpretation that increased Pka activity due to elevated cAMP levels is the cause of the Hh signalling defects in *mthl5* mutants.

PKA phosphorylation stabilizes Smo in Hh-responding cells. Therefore, we checked whether Smo protein levels are elevated in *mthl5* mutant discs. In wild-type discs, Smo shows a complex pattern of post-translational regulation (Fig. 7T): protein levels are high in posterior compartment cells, where Ptc levels (and thus Smo inhibition) are low or absent; higher in anterior cells closest to the A-P boundary where Hh signalling (and Smo phosphorylation) is strongest; low in further anterior Hh-responding cells due to Gprk2-dependent internalization of activated Smo (Cheng et al., 2010); and lowest in far anterior cells beyond the range of Hh diffusion (Denef et al., 2000). In $mthl5^{MB03076}$ mutant discs with an expanded Hh response, we saw a corresponding anterior expansion of Smo stabilization (Fig. 7U,V). Conversely, expression of Mthl5-GFP blocked Smo stabilization in Hh-responding cells at the A-P

Development (2021) 148, dev189258. doi:10.1242/dev.189258

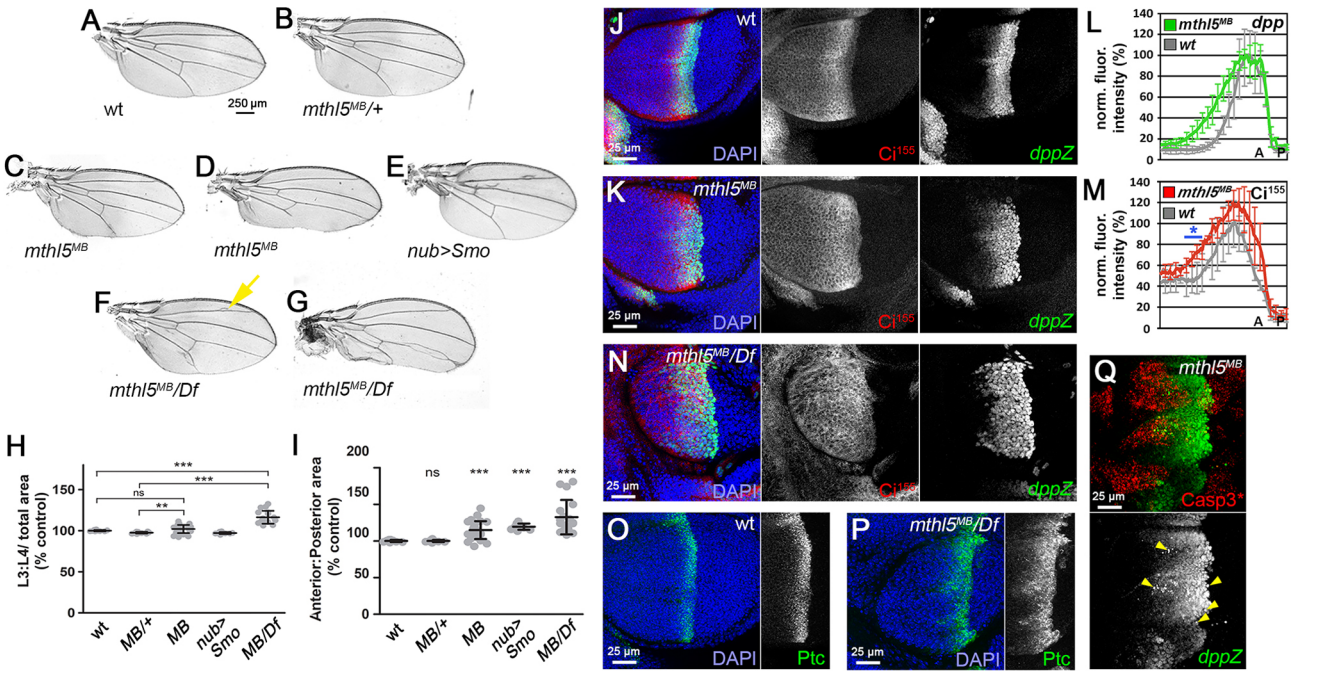

Fig. 5. Hh responsiveness is increased in *mthl5* mutants. (A-I) Wings from control (w^{1118}) (A), $mthl5^{MB03076}$/+ (B), weakly and strongly affected $mthl5^{MB03076}$ (C,D), Smo-GFP-expressing (E), and weakly and strongly affected $mthl5^{MB03076}$/*Df(3R)BSC514* (F,G) flies. Arrow in F indicates ectopic vein. L3-L4:total wing area and A:P area ratios are quantified in H and I, respectively. **P<0.01; ***P<0.001; ns, not significant (unpaired two-tailed *t*-test). All wing images are shown at the same magnification (indicated in A). (J-M) Optical projections of confocal sections from wild-type (w^{1118}) (J) and $mthl5^{MB03076}$ (K) wing discs immunostained using antibodies against Ci^{155} (red) and β-Gal (expressed from a *dpp* enhancer trap; green). DAPI is blue. β-Gal and Ci^{155} fluorescence intensities are quantified in L and M, respectively, data are mean±s.d. from five discs. Blue bar in M indicates a region where all pixel-by-pixel unpaired two-tailed *t*-tests show a significant difference between control and *mthl5* mutants (P<0.05 or P<0.01). (N) Optical projection of confocal sections from a $mthl5^{MB03076}$/*Df(3R)BSC514* disc stained as in J,K. (O,P) Optical projections of confocal sections from wild-type (O) and $mthl5^{MB03076}$ (P) discs immunostained using an antibody against Ptc (green). DAPI is in blue. (Q) Optical projections of confocal sections from a $mthl5^{MB03076}$ wing disc immunostained using antibodies against β-Gal (expressed from a *dpp* enhancer trap; green) and activated caspase 3 (red). Arrowheads indicate β-Gal-positive basal pyknotic nuclei. Compared with 29 control discs (J), phenotypes were seen in 14/32 (*dpp*) and 10/32 (Ci) discs examined (K); and 9/11 (*dpp*) and 8/11 (Ci) discs (N). Compared with nine control discs (O), phenotype was seen in 11/13 discs (P).

boundary (Fig. 7W,X). These results suggest that Mthl5 impinges upon the pathway at or above the level of Smo, well upstream in the cellular response to Hh.

DISCUSSION

Several GPCRs have been implicated in the vertebrate Hh signalling pathway. They share an ability to modulate cAMP levels through Gαs and Gαi, which can alter sensitivity of cells to Hh ligand (Pusapati et al., 2018). Cells can express a large number of GPCRs, suggesting there could be widespread crosstalk between GPCRs and the Hh pathway. However, it remained an unresolved issue whether the ability to affect Hh signalling is restricted to only a few specific GPCRs or is a more general feature of these receptors. Our screen to test the ability of GPCRs expressed in the *Drosophila* wing disc to influence Hh responses indicates that the latter is true. We found that many GPCRs can crosstalk with the Hh pathway – some 45% of those tested in this system. Manipulation of these GPCRs expanded or restricted the domain of Hh responses, consistent with them working to enhance or diminish sensitivity to Hh rather than being strictly required

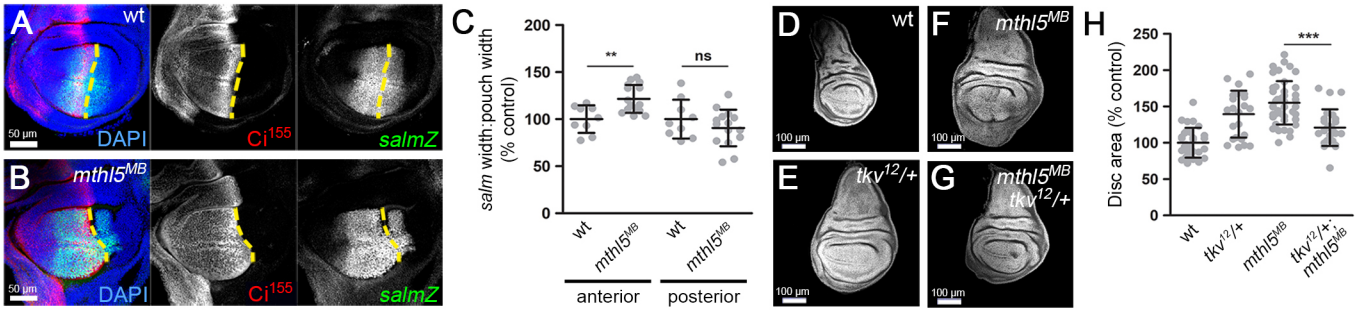

Fig. 6. Anterior expansion of *dpp* expression leads to *mthl5* mutant wing disc overgrowth. (A,B) Wild-type (A) and $mthl5^{MB03076}$ mutant (B) wing discs immunostained using antibodies against Ci^{155} (red) and β-Gal (expressed from a *salm* enhancer trap; green). (C) Quantification of the width of the anterior and posterior *salm* expression domains relative to total wing pouch width. **P<0.01; ns, not significant (unpaired two-tailed *t*-test). Data are pooled from two independent experiments. (D-H) Confocal images of wild-type (D), tkv^{12}/+ (E), $mthl5^{MB03076}$ (F) and tkv^{12}/+;$mthl5^{MB03076}$ (G) wing discs stained with DAPI. Mean disc area is quantified in H; ***P<0.001 (unpaired two-tailed *t*-test). Data are pooled from two independent experiments.

Development (2021) 148, dev189258. doi:10.1242/dev.189258

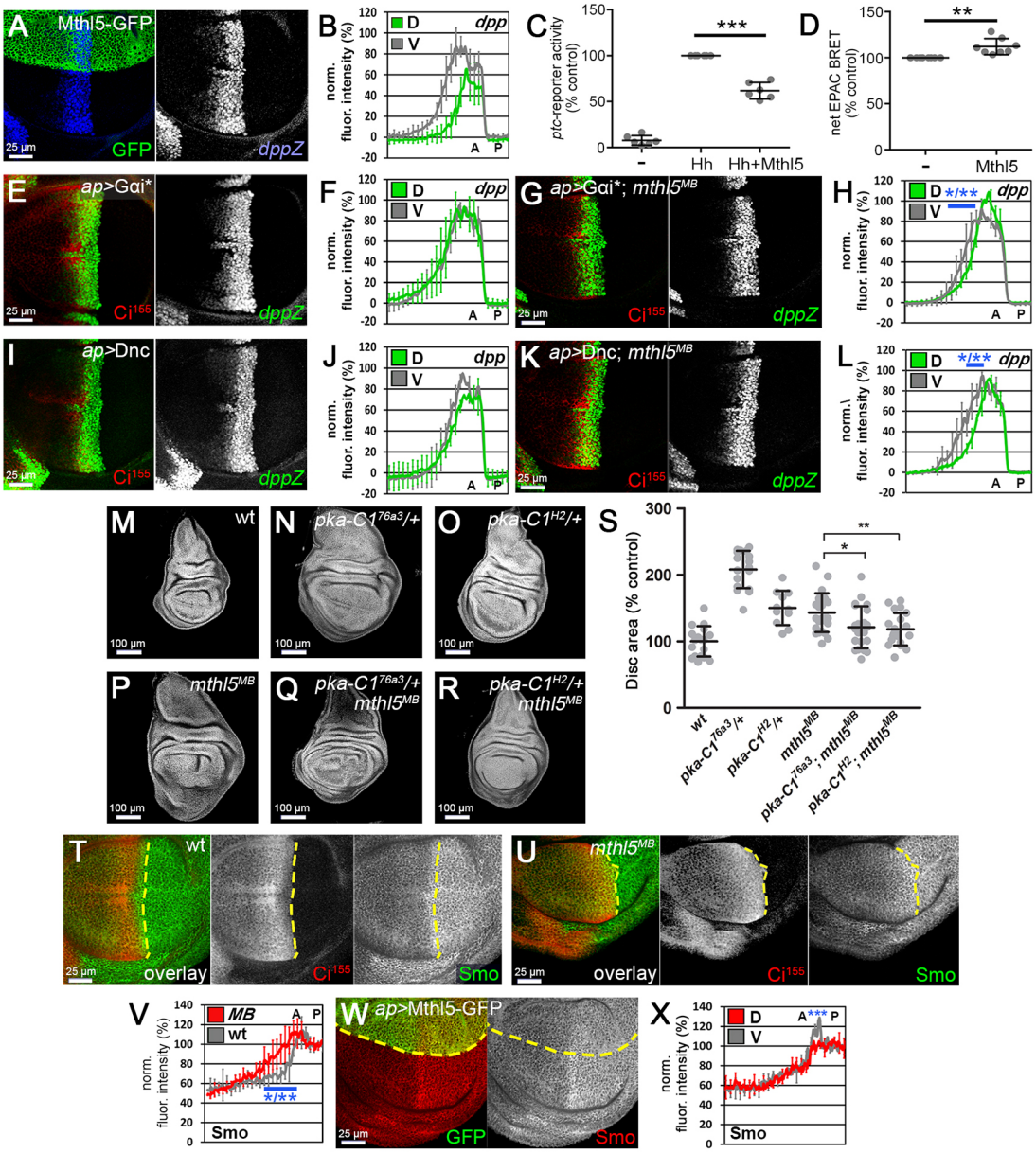

Fig. 7. Hh signalling defects in *mthl5* mutants are caused by cAMP misregulation. (A,B) Wing disc expressing Mthl5-GFP (green) in the dorsal compartment, immunostained using antibody against β-Gal (expressed from a *dpp* enhancer trap; blue). Fluorescence intensities are quantified in B. Data represent the mean±s.d. of five wing discs. (C) *ptc*-luc reporter assay in *Drosophila* S2-R+ cells. Cells were transfected with empty vector (–) or expression plasmids for Mthl5-GFP and/or Hh^N, as indicated. Data are mean±s.d. of six independent experiments. ***P<0.001 (ratio paired two-tailed *t*-test). (D) Measurement of basal cAMP levels by EPAC-BRET assay in mock- and Mthl5-GFP-transfected S2-R+ cells. Graphed data represent the mean±s.d. of eight independent experiments. **P<0.01 (ratio-paired two-tailed *t*-test). (E-L) Wild-type (E,I) or $mthl5^{MB03076}$ (G,K) wing discs expressing proteins expected to lower cAMP levels [activated Gαi (E,G) or the phosphodiesterase Dnc (I,K)] in the dorsal compartment. Discs were immunostained using antibody against Ci^{155} (red) and β-Gal (expressed from a *dpp* enhancer trap; green). Fluorescence intensities are quantified in F,H,J,L; data are mean±s.d. of five discs. Blue bars in H,L indicate regions where all pixel-by-pixel unpaired two-tailed *t*-tests show significant differences between dorsal and ventral compartments with P<0.05 or P<0.01. (M-S) Wild-type (M), $pka\text{-}C1^{76a3}$/+ (N), $pka\text{-}C1^{H2}$/+ (O), $mthl5^{MB03076}$ (P), $pka\text{-}C1^{76a3}$/+; $mthl5^{MB03076}$ (Q) and $pka\text{-}C1^{H2}$/$mthl5^{MB03076}$ (R) discs stained with DAPI. Mean disc areas are quantified in S. *P<0.05; **P<0.01 (unpaired two-tailed *t*-test). The experiment was performed once. (T-V) Wild-type (T) or $mthl5^{MB03076}$ (U) wing discs immunostained using antibodies against Ci^{155} (red) and Smo (green). Yellow dotted lines indicate the A-P boundary. Fluorescence intensities are quantified in V; data are mean±s.d. of five discs. Blue bar indicates region where 71% of pixel-by-pixel unpaired two-tailed *t*-tests show significant difference between wild-type and $mthl5^{MB03076}$ discs (P<0.05 or P<0.01). (W,X) Wing disc expressing Mthl5-GFP (green) in the dorsal compartment (W), immunostained using antibody against Smo (red). Fluorescence intensities are quantified in X; data are mean±s.d. of five wing discs. D is significantly different from V; ***P<0.001 (unpaired two-tailed *t*-test). Phenotypes were seen in 8/15 discs examined (A), in 0/8 discs (E), in 10/18 discs (G), in 5/10 discs (I) in 14 of 20 discs (K), in 8 of 22 discs (U) and in 8/8 discs (W).

components of the pathway. Analysis of mutants for one specific GPCR identified in the screen, Mthl5, provided evidence that this effect on Hh signalling involves modulation of cAMP levels (and thus PKA activity), a factor with a positive effect on Smo activity in *Drosophila*.

GPCRs as attenuators and enhancers of Hh responsiveness

The best-characterized example of a GPCR influencing Hh signalling is GPR161 in mammals. In *Gpr161* mutant mice, the range of expression of the Shh target genes *Nkx2.2* and *Foxa2* in the neural tube is expanded dorsally (Mukhopadhyay et al., 2013). This

Development (2021) 148, dev189258. doi:10.1242/dev.189258

Hh gain-of-function phenotype can be recapitulated in *Gpr161* mutant cultured neural precursor cells, and is accompanied by a three- to fourfold increase in sensitivity to Shh ligand (Pusapati et al., 2018). GPR161 overexpression had the opposite effect, suppressing the response to Shh in cells (Pusapati et al., 2018). This appears to be linked to the ability of GPR161 to activate Gαs and stimulate cAMP production, thereby promoting formation of the GLI3R transcriptional repressor. In this context, GPR161 acts as an attenuator of signalling by modulating how easily activated the pathway is, rather than as a direct inhibitor of signalling.

We saw similar effects from manipulating GPCRs in flies. This was true at the level of Hh-dependent adult wing phenotypes and readouts of Hh pathway activity in discs, including both low (Ci^{155} stabilization and *dpp* expression) and intermediate/high (expression of *ptc*, stabilization of Smo) threshold responses. Most GPCRs fell neatly into two categories. The first consists of four GPCRs – Mthl5, GABA-B-R2, Cirl and Mth. The G protein selectivity of three of these is known, with all coupling to Gαi or Gαo to lower cAMP levels (Franek et al., 1999; Patel et al., 2016; Scholz et al., 2017; Wojcik and Neff, 1984). Depletion of these GPCRs generally expanded the range of Hh responses. This phenocopied Gαi depletion and resembled the effects seen in Gpr161 mutant mouse embryos. The second category contained six GPCRs – Mthl4, Mthl8, Mthl9, Rk, Stan and CG15744. The selectivity of only one of these receptors is known: Rk stimulates cAMP production through Gαs (Baker and Truman, 2002; Kimura et al., 2004). Depletion of these receptors phenocopied Gαs depletion, narrowing the range of *dpp* expression. The match between GPCR and Gα depletion phenotypes for those GPCRs with known coupling specificity provides support for the specificity of our screen results. For both categories of GPCRs, the effects fit nicely with the expectations of attenuators and enhancers of Hh responsiveness, respectively. Loss of Gαi-like receptors, such as Mthl5, allowed cells further from the source of Hh, and thus exposed to lower levels of Hh, to initiate a signalling response, while loss of Gαs-like GPCRs shrank the effective range.

Of the readouts we used, expression of *dpp* produced the most-striking effects, but is not exclusive to the Hh pathway. For example, apoptotic disc cells can upregulate *dpp* in some circumstances (Perez-Garijo et al., 2004; Ryoo et al., 2004), whereas En can repress *dpp* expression (Raftery et al., 1991; Strigini and Cohen, 1997). This raised the possibility that GPCRs could be acting on *dpp* through a different mechanism. With regard to apoptosis, we did not observe any correlation between apoptotic cells and *dpp* expression in *mthl5*-depleted or mutant discs, and the *dpp* expression domain was expanded even in conditions where apoptosis was comparatively low or suppressed. Furthermore, an apoptosis-based mechanism would not explain why *dpp* expression is more restricted in Mthl5-overexpressing discs, or when Gαs or GPCRs like Rk are depleted. Apoptosis thus seems unlikely to be the major driver of the changes we observed. Although failure to activate anterior *en* expression could upregulate *dpp* expression, we observed substantial anterior En expression after depletion of Gαi, Mthl5 or Cirl. Although the levels were slightly lower than normal for unknown reasons, a comparable decrease in anterior En levels was not sufficient to trigger expansion of *dpp* expression in Gαs- or Rk-depleted discs. Although we cannot rule out the possibility that a reduction in anterior En levels could contribute to expansion of *dpp* expression in Gαi-like GPCR-depleted discs, it seems unlikely to be the main cause.

The interpretation that Hh signalling itself is affected is best supported for the Gαi-like GPCRs. Unlike *dpp* expression, stabilization of Smo and Ci^{155}, and expression of Ptc are Hh-specific readouts. In particular, stabilization of Smo and Ci^{155} are proximal readouts of cytoplasmic Hh signalling. Their concomitant upregulation in Gαi-like GPCR-depleted or mutant cells, specifically those within range of the A-P boundary (and a similar effect in discs in which PKA activity is moderately upregulated; Jia et al., 2004) is a good indicator of increased Hh pathway activity. As stabilization of Ci^{155} is sufficient to de-repress *dpp* and enable its expression in response to Hh (Méthot and Basler, 1999), increased Hh-dependent Ci stabilization (and possibly Ci activation) is the most likely explanation for the observed expansion of *dpp* expression. However, given the stronger effects on *dpp* expression than on other Hh pathway readouts, it remains possible that GPCRs affect *dpp* through another mechanism. We also cannot rule out the possibility that GPCRs affect *hh* expression, rather than ligand sensitivity. This is not the case in mice (Pusapati et al., 2018), and the fact that Mthl5 reduced responsiveness to transfected Hh in S2 cells (as did Gαs depletion in our previous work; Praktiknjo et al., 2018) suggests that the effects we see occur downstream of Hh.

How do GPCRs influence Hh signalling activity?

One of the main differences in the effects of GPCR signalling between different systems is that cAMP attenuates Hh pathway activity in mammals but seems to predominantly enhance it in flies. In both systems, cAMP/PKA negatively regulates Hh target gene expression by promoting conversion of Ci/GLI proteins to their repressor forms. However, in *Drosophila* PKA also acts as the gatekeeper for pathway activation by phosphorylating Smo. Although its inhibitory effect on Ci can be inferred in extreme conditions in flies (such as *pka-C1* mutant clones; Li et al., 1995; Ohlmeyer and Kalderon, 1998), the activating function of PKA seems to predominate at physiological levels of cAMP/PKA signalling. This may be because Ci is protected from increased PKA activity as Smo activity increases in fly cells. Specifically, PKA switches from Ci- to Smo-containing complexes in response to Hh, and active Smo promotes release of Ci from the complex that converts it to CiR (Ranieri et al., 2014; Robbins et al., 1997; Ruel et al., 2007).

The evidence suggests that GPCRs are not core components involved in transduction of the Hh signal. Instead, their activity feeds in to shape the response to Hh in tissues, modulating basal cellular cAMP levels to alter thresholds for Hh pathway activation and output (Pusapati et al., 2018). In vertebrate cells, this is thought to be through effects on GLI regulation. The higher the basal cellular levels of cAMP and PKA activity are, the more likely that GLI proteins are converted to their repressor forms. For a given level of target gene expression, overcoming this increased activation threshold requires stronger Hh pathway activity, meaning exposure to a higher concentration of Shh. Ligand sensitivity is thus attenuated by cAMP, which narrows the range over which target genes are expressed. However, in *Drosophila* cells the higher basal cellular levels of cAMP and PKA activity are, the lower the barrier to Smo activation. The pathway should thus be activated at lower ligand concentrations, which would expand the range over which target genes are expressed. It makes sense that modulating ligand sensitivity in this way would have the strongest effects in cells exposed to the lowest and most-limiting Hh levels. Consistent with this, the strongest changes we observed in both Gαs- and Gαi-like GPCR-depleted discs were in *dpp*-expressing cells farther from the source of Hh.

Mthl5 is a novel attenuator of Hh signalling

We identified the little-characterized GPCR Mthl5 as a novel attenuator of Hh signalling in discs. *mthl5* mutants showed clear

Development (2021) 148, dev189258. doi:10.1242/dev.189258

signs of Hh pathway upregulation, including anterior compartment overgrowth and increased L3-L4 spacing in wings, and anterior expansion of Smo and Ci^{155} protein stabilization and Hh target gene expression. Overexpression of Mthl5 had the opposite effect, restricting the domain of *dpp* expression. Mthl5 likely crosstalks with the Hh pathway by coupling to inhibitory Gα subunits and decreasing cellular cAMP levels. This is supported by the similarity of *mthl5* and *gαi* depletion phenotypes, the ability of Mthl5 expression to lower cAMP levels and *ptc*-reporter activity in S2 cells, and the partial rescue of *mthl5* mutant defects by lowering cAMP or PKA levels.

The anterior expansion of *dpp* expression in *mthl5* mutants caused a corresponding shift in Dpp signalling activity, as evidenced by an increase in the width of the anterior expression domain of *salm*. Cells in both the wing pouch and the pleura are dependent on low-level activation of Dpp signalling for growth (Barrio and Milán, 2017). We imagine that the anterior expansion of *dpp* expression could lead to excessive proliferation of cells in the anterior lateral and hinge region of the discs, which could in part account for overgrowth in *mthl5* mutant discs, although this remains to be confirmed.

Physiological importance of extensive GPCR-Hh crosstalk

Our results demonstrate that crosstalk of GPCR signalling with Hh signalling is conserved from flies to vertebrates, and suggest that there may be many more vertebrate GPCRs that are capable of doing this. The cilium, which plays a central organizing role in vertebrate Hh signalling (Bangs and Anderson, 2017), may act as an insulator against this sort of crosstalk by compartmentalizing cAMP responses for some GPCRs (Marley et al., 2013). Although it remains to be tested, this crosstalk could be a specific mechanism for linking the myriad stimuli that activate GPCRs – mechanical force for Cirl (Scholz et al., 2017), planar polarity cues for Stan (Usui et al., 1999), a nutrient-regulated peptide for Mth (Delanoue et al., 2016) and a glycoprotein hormone marking developmental timing for Rk (Loveall and Deitcher, 2010) – to developmental patterning and tissue homeostasis. Further work will be needed to determine the links between the physiological regulators of these GPCRs and Hh pathway output.

MATERIALS AND METHODS

Drosophila strains and culture

For crosses involving RNAi transgene expression, RNAi transgenic males were crossed to *w,UAS-Dcr;nub-Gal4* females (for adult wings) or *w,UAS-Dcr;ap-Gal4,dpp^{10638}/CyO,Kr-Gal4,UAS-GFP* females (for discs) at 25°C for 2 to 3 days and the resulting offspring were transferred to 27°C until dissection or hatching. All other crosses were carried out at 25°C. For crosses where we analysed growth (Figs 4D-F, 5A-G, 6D-G, 7M-R) or directly compared Hh responses in *mthl5* mutants and wild-type discs (Figs 5J,K,O,P, 6A,B, 7T,U), crosses were handled in parallel batches and flipped regularly to avoid crowding of the larvae. The following strains were used: *UAS-Dcr-2.D*, *UAS-P35*, *nub-GAL4*, *ap-GAL4*, *dpp^{10638}* (*dpp-LacZ*), *salm^{03602}* (*salm-LacZ*), *mthl5^{MB03076}*, *Df(3R)BSC514*, *UAS-Dnc*, *tkv^{12}*, *pka-C1^{H2}* and *pka-C1^{76a3}* [all obtained from the Bloomington Drosophila Stock Centre (BDSC)]; *UAS-gαi.dsRNA* and *UAS-Gαi^{Q205L}* (Schaefer et al., 2001) [generously provided by J. Knoblich (Institute of Molecular Biotechnology, Vienna, Austria)]. A list of transgenic RNAi strains obtained from the Vienna Drosophila Resource Centre (indicated by a 'V') or from the Transgenic RNAi Project via the BDSC (indicated by 'TRiP') and used in this study can be found in Table S2.

The *mthl5^{MB03076}* strain contains an insertion of a *Minos* element in coding exon 5 of the *mthl5* gene, at position 3R:11,884,499. We validated the insertion by amplifying both the 5′ and 3′ flanking regions, using the following primer pairs: Minos 5′ (5′-cttcatctttcaggaggcttg-3′)+*mthl5* exon 6 (5′-gacattactaacagcatcagcg-3′); Minos 3′ (5′-ggagttcttcgcccaccc-3′) plus *mthl5* exon 4 (5′-gctccgcaaaatcttaaaccc-3′). The resultant PCR products were cloned into pGEM according to manufacturer's instructions and sequenced to confirm the correct insertion site. The *w^{1118};mthl5^{MB03076}/TM3* stock we obtained from Bloomington had a background lethal mutation on the third chromosome, which we removed by recombination.

To generate Mthl5-GFP expression vectors, the Mthl5 open reading frame was PCR amplified from cDNA in two overlapping fragments. The 5′ fragment from nucleotides 1 to 738 of the coding sequence was amplified to introduce an EcoRI site immediately upstream of the start codon (primers 5′-gaattcatgctcgtaaaaacgcttgg-3′ and 5′-cgttgtcacaatgttaccaacc-3′). The 3′ fragment from nucleotides 721 to 1488 of the coding sequence was amplified to replace the stop codon with a NotII site (primers 5′-cctactctcagagatctggttgg-3′ and 5′-gcggccgcgtaatcgttgccgttcatataa-3′). Each PCR product was cloned into pGEM. The 5′ fragment was then excised using EcoRI and BglII, which cuts *mthl5* at coding sequence nucleotide 732. The 3′ fragment was excised using BglII and NotI. These two fragments were then cloned together with a NotI-KpnI fragment encoding GFP into *pMT.puro* for expression in cell culture. The full-length sequence was then excised as an EcoRI-KpnI fragment and transferred into pUAST. Transgenic flies carrying pUAST/Mthl5-GFP were generated by BestGene.

Genotypes

The following genotypes are shown in each figure: Fig. 1A, *w,UAS-Dcr/w;nub-GAL4/+*; Fig. 1B, *w,UAS-Dcr/w;nub-GAL4/+;UAS-gαs-IR$^{TRiP.HMC03106}$/+*; Fig. 1C, *w,UAS-Dcr/w;nub-GAL4/UAS-gαi-IR*; Fig. 1E, *w,UAS-Dcr/w;nub-GAL4/UAS-mthl6-IR^{V108048}*; Fig. 1F, *w,UAS-Dcr/w;nub-GAL4/UAS-mthl8-IR^{V100246}*; Fig. 1G, *w,UAS-Dcr/w;nub-GAL4/UAS-mthl9-IR^{V108967}*; Fig. 1H, *w,UAS-Dcr/w;nub-GAL4/UAS-rk-IR^{V105360}*; Fig. 1I, *w,UAS-Dcr/w;;nub-GAL4/UAS-rk-IR^{V905}*; Fig. 1J, *w,UAS-Dcr/w;nub-GAL4/+;UAS-cg15744-IR^{V4801}/+*; Fig. 1K, *w,UAS-Dcr/w;nub-GAL4/UAS-mthl4-IR^{V50752}*; Fig. 1L, *w,UAS-Dcr/w;nub-GAL4/UAS-stan-IR^{V107993}*; Fig. 1N, *w,UAS-Dcr/w;nub-GAL4/UAS-mthl5-IR^{V101593}*; Fig. 1O, *w,UAS-Dcr/w;nub-GAL4/UAS-gaba-b-r2-IR^{V1785}*; Fig. 1P, *w,UAS-Dcr/w;nub-GAL4/+;UAS-gaba-b-r2-IR$^{TRiP.JF02779}$/+*; Fig. 1Q, *w,UAS-Dcr/w;nub-GAL4/UAS-cirl-IR^{V100749}*; Fig. 1R, *w,UAS-Dcr/w;nub-GAL4/UAS-mth-IR^{V102303}*; Fig. 2A, *w,UAS-Dcr/w;ap-GAL4,dpp^{106346}/+*; Fig. 2C, *w,UAS-Dcr/w;ap-GAL4,dpp^{106346}/+;UAS-gαs-IR$^{TRiP.HMC03106}$/+*; Fig. 2E, *w,UAS-Dcr/w;ap-GAL4,dpp^{106346}/UAS-mthl4-IR^{V50752}*; Fig. 2G, *w,UAS-Dcr/w;ap-GAL4,dpp^{106346}/UAS-mthl8-IR^{V100246}*; Fig. 2I, *w,UAS-Dcr/w;ap-GAL4,dpp^{106346}/UAS-mthl9-IR^{V108967}*; Fig. 2K, *w,UAS-Dcr/w;ap-GAL4,dpp^{106346}/UAS-rk-IR^{V905}*; Fig. 2M, *w,UAS-Dcr/w;ap-GAL4,dpp^{106346}/+;UAS-cg15744-IR^{V4801}/+*; Fig. 2O, *w,UAS-Dcr/w;ap-GAL4,dpp^{106346}/UAS-stan-IR^{V107993}*; Fig. 3A, *w,UAS-Dcr/w;ap-GAL4,dpp^{106346}/UAS-gαi-IR*; Fig. 3C, *w,UAS-Dcr/w;ap-GAL4,dpp^{106346}/UAS-mthl5-IR^{V101593}*; Fig. 3E, *w,UAS-Dcr/w;ap-GAL4,dpp^{106346}/UAS-gaba-b-r2-IR^{V1785}*; Fig. 3G, *w,UAS-Dcr/w;ap-GAL4,dpp^{106346}/UAS-mth-IR^{V102303}*; Fig. 3I, *w,UAS-Dcr/w;ap-GAL4,dpp^{106346}/UAS-cirl-IR^{V100749}*; Figs 4A,B,D, 5A,O, 6D, 7M,T, *w^{1118}*; Figs 4E,I, 5C,D, 6F, 7P,U, *w;;mthl5^{MB03076}/mthl5^{MB03076}*; Figs 4F,J, 5F,G,P, *w;;mthl5^{MB03076}/Df(3R)BSC514*; Fig. 5B, *w;;mthl5^{MB03076}/+*; Fig. 5E, *w,UAS-Dcr/w;nub-GAL4/UAS-smo3′UTR-dsRNA;UAS-Smo-GFP/+*; Fig. 5J, *w;dpp^{106346}/+*; Fig. 5K,Q, *w;dpp^{106346}/+;mthl5^{MB03076}/mthl5^{MB03076}*; Fig. 5N, *w;dpp^{106346}/+;mthl5^{MB03076}/Df(3R)BSC514*; Fig. 6A, *w;salm^{03602}/+*; Fig. 6B, *w;salm^{03602}/+;mthl5^{MB03076}/mthl5^{MB03076}*; Fig. 6E, *w;tkv^{12},FRT40/+*; Fig. 6G, *w;tkv^{12},FRT40/+;mthl5^{MB03076}/mthl5^{MB03076}*; Fig. 7A,W, *w;ap-GAL4,dpp^{106346}/+;UAS-Mthl5-GFP/+*; Fig. 7E, *w;ap-GAL4,dpp^{106346}/UAS-Gαi^{Q205L}*; Fig. 7G, *w;ap-GAL4,dpp^{106346}/UAS-Gαi^{Q205L};mthl5^{MB03076}/mthl5^{MB03076}*; Fig. 7I, *w;ap-GAL4,dpp^{106346}/UAS-Dnc*; Fig. 7K, *w;ap-GAL4,dpp^{106346}/UAS-Dnc;mthl5^{MB03076}/mthl5^{MB03076}*; Fig. 7N, *w;pka-C1^{76a3}/+*; Fig. 7O, *w;pka-C1^{H2}/+*; Fig. 7Q, *w;pka-C1^{76a3}/+;mthl5^{MB03076}/mthl5^{MB03076}*; and Fig. 7R, *w;pka-C1^{H2}/+; mthl5^{MB03076}/mthl5^{MB03076}*.

Generation of anti-Mthl5 antiserum

A rabbit polyclonal antiserum against the Mthl5 extracellular N terminus was generated at Genscript. A bacterially expressed fusion protein consisting of Mthl5 amino acids 24-219 (lacking the N-terminal signal peptide) fused to a 6xHis tag was used as the immunogen.

Development (2021) 148, dev189258. doi:10.1242/dev.189258

RNAseq analysis of third instar wing discs

Wing discs were dissected in PBS from third instar larvae of the genotype *w;apGAL4/+* and transferred individually in a minimal volume of PBS using forceps to a microcentrifuge tube on ice. After 20 min of collecting, the tubes were snap-frozen and stored at −70°C. Total RNA was isolated from 100-120 imaginal discs per sample using TRIzol reagent (ThermoFisher Scientific). RNA was quantified using a Nanodrop spectrophotometer and quality was assessed using a 2100 Bioanalyzer instrument (Agilent Technologies). Three independent RNA preparations were submitted to the IRCM Molecular Biology Core Facility for library preparation. Libraries were pair-end sequenced at Genome Quebec using a HiSeq2000 platform. Bioinformatic analysis was performed by the IRCM Bioinformatics Core Facility. Raw reads (26-28 million per sample) were filtered for quality (using FastQC, phred33 score>30) and aligned to the dm3 reference genome using TopHat2, yielding per-gene sequence read counts.

Dissection, immunostaining, confocal microscopy and image analysis

Wandering third instar larvae were dissected, and the imaginal discs fixed and processed for immunostaining as previously described (Maier et al., 2014). For comparisons of Hh responses in *mthl5* mutants and wild-type discs (Figs 5J,K,O,P, 6A,B, 7T,U), crosses for comparison were handled, dissected and processed for immunostaining in parallel batches, and discs imaged using the same confocal settings. Antibodies used for immunostaining were: rabbit anti-β-galactosidase (A11132, 1:1000; Thermo Fisher Scientific), rat anti-Ci^{155} [2A1, 1:50; Developmental Studies Hybridoma Bank (DSHB), Iowa City, IA, USA], mouse anti-Ptc (Apa-1, 1:1000; DSHB), rabbit anti-cleaved caspase 3 (Asp 175, 1:200; Cell Signaling Technologies), mouse anti-Wg (4D4, 1:25; DSHB) and rabbit anti-Mthl5 (1:1000; this study; Fig. S2). Image stacks of the discs were taken using a Zeiss LSM700 confocal microscope. Quantification of fluorescence intensity was carried out using Image J. For dorsal versus ventral compartment comparisons, measurements were made in equal-sized rectangles spanning the A-P boundary in dorsal and ventral regions of each wing disc image using the Plot Profile function. For Ci^{155} and Hh target genes, dorsal and ventral data were normalized by dividing each value by the average of the 10 highest intensity values from the ventral (wild-type) compartment within the same disc, effectively converting them to the percentage of maximum wild-type response. For En and Smo, data were normalized to the mean fluorescence intensity in the wild-type ventral posterior compartment. For comparisons between *mthl5* mutants and wild-type discs (Figs 5J,K,O,P, 6A,B, 7T,U), measurements were made in a single box of uniform size spanning the D-V boundary and data were normalized to the average maximal mean fluorescence intensity in the wild-type discs (for target genes and Ci^{155}) or the average posterior compartment fluorescence (for Smo). Data from five discs were arranged to align the A-P boundaries and pixel-by-pixel data averaged to yield a mean intensity plot±s.d. along the A-P axis. Quantification of the total size of the imaginal disc was performed using ImageJ by tracing the outlines of DAPI-stained discs using the Polygon tool and measuring the outlined area with the Measurement tool. To measure wing pouch size, a line spanning the folds at the posterior and anterior limits of the pouch was drawn at the midline of the wing pouch using the Straight line tool, and its length measured with the Measurement tool. For estimating the anterior and posterior extents of *salm* expression, a straight line spanning the A-P boundary to the anterior or posterior limit of *salm-LacZ* expression was drawn along the midline of the pouch and measured. These values were divided by the total pouch length to correct for any small differences in disc size, although similar results were obtained without normalization. Statistical significance was determined using an unpaired two-tailed Student's *t*-test.

Analysis of adult wings

Adult flies were collected and stored in 50% ethanol/50% glycerol. Before mounting, they were rinsed with water. Wings were then dissected in water and transferred into a drop of Faure's solution on a glass slide and cover-slipped. A weight was placed on the cover slip to flatten the wings and they were left to dry overnight. Wings were imaged with a Leica DM2000 light microscope. Wings areas were measured by outlining the appropriate region (whole wing, L3-L4 area, from L4 to the anterior margin to approximate anterior compartment and from L4 to the posterior margin to approximate posterior compartment) using the Polygon selection tool of Image J. The area of the resulting polygon was calculated using the Measure tool.

BRET and ptc-Luciferase reporter assays

EPAC-BRET assays were performed as previously described (Maier et al., 2014). Briefly, 1×10^6 S2R+ cells [obtained from the Drosophila Genomics Resource Center (DGRC)] were plated in 0.5 ml of serum-free Schneider's medium in 24-well plates on day 1. A few hours later, they were transfected with 100 ng of *pMT.puro/Mthl5-GFP* or empty *pMT.puro* vector (control), together with 250 ng of the EPAC-cAMP biosensor-encoding plasmid *pMT.puro/GFP10-EPAC-RLucII_T781A,F782A*. Transgene expression was induced on day 2 by adding $CuSO_4$ to a concentration of 0.5 mM. On day 4, the cells were harvested, washed once with PBS and split into four wells of a white walled, clear-bottom 96-well plate. Substrate was added and emissions at 400 nm (RLucII, donor) and 515 nm (GFP10, acceptor) measured and corrected for background as described previously (Cheng et al., 2012). The net BRET signal was calculated as the ratio of background corrected GFP10: RLucII emission. Quadruplicate readings for each condition were averaged, and the experiment performed eight times. Statistical significance of the difference in the compiled experimental averages for each condition was assessed using a ratio-paired *t*-test in GraphPad Prism. This test controls for inter-experimental variability in the magnitude of the raw reads. Data were then normalized to the mock-transfected control (=100%) within each experiment to generate graphs.

ptc-Luciferase reporter assays were performed as previously described (Maier et al., 2014). Briefly, cells were plated as above and co-transfected with 100 ng *pMT/Ci*, 75 ng *pGL.basic/ptcD136-luc* (Chen et al., 1999), 75 ng *pRL/CMV* and 100 ng of each additional expression plasmid (*pMT.puro/*Hh^N, *pMT.puro/Mthl5-GFP* or *pMT.puro* vector as control). Cells were induced and split as above. On day 4, luciferase activity measurements were performed as described previously (Maier et al., 2014). Quadruplicate readings for each condition were averaged, and the experiment performed six times. Statistical significance of the difference in the compiled experimental averages for each condition was assessed using a ratio-paired *t*-test in GraphPad Prism. Data were then normalized to the mean Hh response (+Hh condition=100%) within each experiment to generate graphs.

Mthl5 secondary structure prediction

In silico prediction of the transmembrane helices in Mthl5 protein was performed using the TMHMM Server v. 2.0 (http://www.cbs.dtu.dk/services/TMHMM/).

Acknowledgements

We thank Karen Oh for expert technical assistance, Dhara Patel for her early contribution to the project and Dr Virginie Calderon of the IRCM Bioinformatics Core Facility for preparing the heat map of GPCR expression. Fly stocks obtained from the Bloomington Drosophila Stock Center (supported by NIH grant P40OD018537) were used in this study, as were antibodies from the Developmental Studies Hybridoma Bank (created by the NICHD, National Institutes of Health, and maintained at The University of Iowa, Department of Biology, Iowa City, IA 52242) and cells from the DGRC (Drosophila Genomics Resource Center; supported by NIH grant 2P40OD010949).

Competing interests

The authors declare no competing or financial interests.

Author contributions

Conceptualization: D.R.H.; Methodology: F.S., D.R.H.; Validation: F.S., D.R.H.; Formal analysis: F.S., D.R.H.; Investigation: F.S.; Writing - original draft: F.S., D.R.H.; Writing - review & editing: F.S., D.R.H.; Visualization: F.S.; Supervision: D.R.H.; Funding acquisition: D.R.H.

Funding

This work was supported by Canadian Institutes of Health Research (106426 to D.R.H.).

Data availability

The RNAseq data discussed in this paper have been deposited in GEO under accession number GSE169490.

Supplementary information

Supplementary information available online at
https://dev.biologists.org/lookup/doi/10.1242/dev.189258.supplemental

Peer review history

The peer review history is available online at
https://journals.biologists.com/dev/article-lookup/148/7/dev189258/

References

Apionishev, S., Katanayeva, N. M., Marks, S. A., Kalderon, D. and Tomlinson, A. (2005). Drosophila Smoothened phosphorylation sites essential for Hedgehog signal transduction. *Nat. Cell Biol.* **7**, 86-92. doi:10.1038/ncb1210

Aza-Blanc, P., RamírezWeber, F.-A., Laget, M.-P., Schwartz, C. and Kornberg, T. B. (1997). Proteolysis that is inhibited by Hedgehog targets Cubitus interruptus protein to the nucleus and converts it to a repressor. *Cell* **89**, 1043-1053. doi:10.1016/S0092-8674(00)80292-5

Baker, J. D. and Truman, J. W. (2002). Mutations in the Drosophila glycoprotein hormone receptor, rickets, eliminate neuropeptide-induced tanning and selectively block a stereotyped behavioral program. *J. Exp. Biol.* **205**, 2555-2565.

Bangs, F. and Anderson, K. V. (2017). Primary Cilia and mammalian Hedgehog signalling. *Cold Spring Harb. Perspect. Biol.* **9**, a028175. doi:10.1101/cshperspect.a028175

Barrio, L. and Milán, M. (2017). Boundary Dpp promotes growth of medial and lateral regions of the Drosophila wing. *eLife* **6**, e22013. doi:10.7554/eLife.22013

Briscoe, J. and Small, S. (2015). Morphogen rules: design principles of gradient-mediated embryo patterning. *Development* **142**, 3996-4009. doi:10.1242/dev.129452

Briscoe, J. and Thérond, P. P. (2013). The mechanisms of Hedgehog signalling and its roles in development and disease. *Nat. Rev. Mol. Cell Biol.* **14**, 416-429. doi:10.1038/nrm3598

Chen, X. and Ganetzky, B. (2012). A neuropeptide signalling pathway regulates synaptic growth in Drosophila. *J. Cell Biol.* **196**, 529-543. doi:10.1083/jcb.201109044

Chen, C.-H., von Kessler, D. P., Park, W., Wang, B., Ma, Y. and Beachy, P. A. (1999). Nuclear trafficking of Cubitus interruptus in the transcriptional regulation of Hedgehog target gene expression. *Cell* **98**, 305-316. doi:10.1016/S0092-8674(00)81960-1

Chen, Y., Sasai, N., Ma, G., Yue, T., Jia, J., Briscoe, J. and Jiang, J. (2011). Sonic Hedgehog dependent phosphorylation by CK1α and GRK2 is required for ciliary accumulation and activation of smoothened. *PLoS Biol.* **9**, e1001083. doi:10.1371/journal.pbio.1001083

Cheng, S., Maier, D., Neubueser, D. and Hipfner, D. R. (2010). Regulation of smoothened by Drosophila G-protein-coupled receptor kinases. *Dev. Biol.* **337**, 99-109. doi:10.1016/j.ydbio.2009.10.014

Cheng, S., Maier, D. and Hipfner, D. R. (2012). Drosophila G-protein-coupled receptor kinase 2 regulates cAMP-dependent Hedgehog signaling. *Development* **139**, 85-94. doi:10.1242/dev.068817

Cohen, J. R., Resnick, D. Z., Niewiadomski, P., Dong, H., Liau, L. M. and Waschek, J. A. (2010). Pituitary adenylyl cyclase activating polypeptide inhibits gli1 gene expression and proliferation in primary medulloblastoma derived tumorsphere cultures. *BMC Cancer* **10**, 676. doi:10.1186/1471-2407-10-676

Davis, R. L. and Kiger, J. A.Jr (1981). Dunce mutants of Drosophila melanogaster: mutants defective in the cyclic AMP phosphodiesterase enzyme system. *J. Cell Biol.* **90**, 101-107. doi:10.1083/jcb.90.1.101

de Celis, J. F. (1998). Positioning and differentiation of veins in the Drosophila wing. *Int. J. Dev. Biol.* **42**, 335-343.

de Celis, J. F., Barrio, R. and Kafatos, F. C. (1996). A gene complex acting downstream of dpp in Drosophila wing morphogenesis. *Nature* **381**, 421-424. doi:10.1038/381421a0

Delanoue, R., Meschi, E., Agrawal, N., Mauri, A., Tsatskis, Y., McNeill, H. and Leopold, P. (2016). Drosophila insulin release is triggered by adipose Stunted ligand to brain Methuselah receptor. *Science* **353**, 1553-1556. doi:10.1126/science.aaf8430

Denef, N., Neubüser, D., Perez, L. and Cohen, S. M. (2000). Hedgehog induces opposite changes in turnover and subcellular localization of patched and smoothened. *Cell* **102**, 521-531. doi:10.1016/S0092-8674(00)00056-8

Fan, J., Liu, Y. and Jia, J. (2012). Hh-induced Smoothened conformational switch is mediated by differential phosphorylation at its C-terminal tail in a dose- and position-dependent manner. *Dev. Biol.* **366**, 172-184. doi:10.1016/j.ydbio.2012.04.007

Franek, M., Pagano, A., Kaupmann, K., Bettler, B., Pin, J. P. and Blahos, J. (1999). The heteromeric GABA-B receptor recognizes G-protein alpha subunit C-termini. *Neuropharmacology* **38**, 1657-1666. doi:10.1016/S0028-3908(99)00135-5

Hanlon, C. D. and Andrew, D. J. (2015). Outside-in signalling–a brief review of GPCR signaling with a focus on the Drosophila GPCR family. *J. Cell Sci.* **128**, 3533-3542. doi:10.1242/jcs.175158

He, X., Zhang, L., Chen, Y., Remke, M., Shih, D., Lu, F., Wang, H., Deng, Y., Yu, Y., Xia, Y. et al. (2014). The G protein α subunit Gαs is a tumor suppressor in Sonic hedgehog-driven medulloblastoma. *Nat. Med.* **20**, 1035-1042. doi:10.1038/nm.3666

Hui, C.-C. and Angers, S. (2011). Gli proteins in development and disease. *Annu. Rev. Cell Dev. Biol.* **27**, 513-537. doi:10.1146/annurev-cellbio-092910-154048

Iglesias-Bartolome, R., Torres, D., Marone, R., Feng, X., Martin, D., Simaan, M., Chen, M., Weinstein, L. S., Taylor, S. S., Molinolo, A. A. et al. (2015). Inactivation of a Galpha(s)-PKA tumour suppressor pathway in skin stem cells initiates basal-cell carcinogenesis. *Nat. Cell Biol.* **17**, 793-803. doi:10.1038/ncb3164

Ingham, P. W., Nystedt, S., Nakano, Y., Brown, W., Stark, D., van den Heuvel, M. and Taylor, A. M. (2000). Patched represses the Hedgehog signalling pathway by promoting modification of the Smoothened protein. *Curr. Biol.* **10**, 1315-1318. doi:10.1016/S0960-9822(00)00755-7

Jia, J., Tong, C., Wang, B., Luo, L. and Jiang, J. (2004). Hedgehog signalling activity of Smoothened requires phosphorylation by protein kinase A and casein kinase I. *Nature* **432**, 1045-1050. doi:10.1038/nature03179

Jiang, J. and Hui, C.-C. (2008). Hedgehog signaling in development and cancer. *Dev. Cell* **15**, 801-812. doi:10.1016/j.devcel.2008.11.010

Jiang, L. I., Collins, J., Davis, R., Lin, K.-M., DeCamp, D., Roach, T., Hsueh, R., Rebres, R. A., Ross, E. M., Taussig, R. et al. (2007). Use of a cAMP BRET sensor to characterize a novel regulation of cAMP by the sphingosine 1-phosphate/G13 pathway. *J. Biol. Chem.* **282**, 10576-10584. doi:10.1074/jbc.M609695200

Kimura, K.-I., Kodama, A., Hayasaka, Y. and Ohta, T. (2004). Activation of the cAMP/PKA signalling pathway is required for post-ecdysial cell death in wing epidermal cells of Drosophila melanogaster. *Development* **131**, 1597-1606. doi:10.1242/dev.01049

Klein, R. S., Rubin, J. B., Gibson, H. D., DeHaan, E. N., Alvarez-Hernandez, X., Segal, R. A. and Luster, A. D. (2001). SDF-1 alpha induces chemotaxis and enhances Sonic hedgehog-induced proliferation of cerebellar granule cells. *Development* **128**, 1971-1981.

Langenhan, T., Aust, G. and Hamann, J. (2013). Sticky signalling–adhesion class G protein-coupled receptors take the stage. *Sci. Signal.* **6**, re3. doi:10.1126/scisignal.2003825

Li, W., Ohlmeyer, J. T., Lane, M. E. and Kalderon, D. (1995). Function of protein kinase A in hedgehog signal transduction and Drosophila imaginal disc development. *Cell* **80**, 553-562. doi:10.1016/0092-8674(95)90509-X

Loveall, B. J. and Deitcher, D. L. (2010). The essential role of bursicon during Drosophila development. *BMC Dev. Biol.* **10**, 92. doi:10.1186/1471-213X-10-92

Maier, D., Cheng, S., Faubert, D. and Hipfner, D. R. (2014). A broadly conserved g-protein-coupled receptor kinase phosphorylation mechanism controls Drosophila smoothened activity. *PLoS Genet.* **10**, e1004399. doi:10.1371/journal.pgen.1004399

Marks, S. A. and Kalderon, D. (2011). Regulation of mammalian Gli proteins by Costal 2 and PKA in Drosophila reveals Hedgehog pathway conservation. *Development* **138**, 2533-2542. doi:10.1242/dev.063479

Marley, A., Choy, R. W.-Y. and von Zastrow, M. (2013). GPR88 reveals a discrete function of primary cilia as selective insulators of GPCR cross-talk. *PLoS ONE* **8**, e70857. doi:10.1371/journal.pone.0070857

Martin, F. A., Perez-Garijo, A. and Morata, G. (2009). Apoptosis in Drosophila: compensatory proliferation and undead cells. *Int. J. Dev. Biol.* **53**, 1341-1347. doi:10.1387/ijdb.072447fm

Méthot, N. and Basler, K. (1999). Hedgehog controls limb development by regulating the activities of distinct transcriptional activator and repressor forms of Cubitus interruptus. *Cell* **96**, 819-831. doi:10.1016/S0092-8674(00)80592-9

Mukhopadhyay, S., Wen, X., Ratti, N., Loktev, A., Rangell, L., Scales, S. J. and Jackson, P. K. (2013). The ciliary G-protein-coupled receptor Gpr161 negatively regulates the Sonic hedgehog pathway via cAMP signaling. *Cell* **152**, 210-223. doi:10.1016/j.cell.2012.12.026

Mullor, J. L., Calleja, M., Capdevila, J. and Guerrero, I. (1997). Hedgehog activity, independent of decapentaplegic, participates in wing disc patterning. *Development* **124**, 1227-1237.

Niewiadomski, P., Zhujiang, A., Youssef, M. and Waschek, J. A. (2013). Interaction of PACAP with Sonic hedgehog reveals complex regulation of the hedgehog pathway by PKA. *Cell. Signal.* **25**, 2222-2230. doi:10.1016/j.cellsig.2013.07.012

Niewiadomski, P., Kong, J. H., Ahrends, R., Ma, Y., Humke, E. W., Khan, S., Teruel, M. N., Novitch, B. G. and Rohatgi, R. (2014). Gli protein activity is controlled by multisite phosphorylation in vertebrate Hedgehog signaling. *Cell Rep.* **6**, 168-181. doi:10.1016/j.celrep.2013.12.003

Ogden, S. K., Fei, D. L., Schilling, N. S., Ahmed, Y. F., Hwa, J. and Robbins, D. J. (2008). G protein Gαi functions immediately downstream of Smoothened in Hedgehog signalling. *Nature* **456**, 967-970. doi:10.1038/nature07459

Ohlmeyer, J. T. and Kalderon, D. (1998). Hedgehog stimulates maturation of Cubitus interruptus into a labile transcriptional activator. *Nature* **396**, 749-753. doi:10.1038/25533

Patel, M. V., Hallal, D. A., Jones, J. W., Bronner, D. N., Zein, R., Caravas, J., Husain, Z., Friedrich, M. and Vanberkum, M. F. (2012). Dramatic expansion and developmental expression diversification of the methuselah gene family during recent Drosophila evolution. *J. Exp. Zool. B Mol. Dev. Evol.* **318**, 368-387. doi:10.1002/jez.b.22453

Patel, M. V., Zhu, J.-Y., Jiang, Z., Richman, A., VanBerkum, M. F. A. and Han, Z. (2016). Gia/Mthl5 is an aorta specific GPCR required for Drosophila heart tube morphology and normal pericardial cell positioning. *Dev. Biol.* **414**, 100-107. doi:10.1016/j.ydbio.2016.03.009

Perez-Garijo, A., Martin, F. A. and Morata, G. (2004). Caspase inhibition during apoptosis causes abnormal signalling and developmental aberrations in Drosophila. *Development* **131**, 5591-5598. doi:10.1242/dev.01432

Perez-Garijo, A., Shlevkov, E. and Morata, G. (2009). The role of Dpp and Wg in compensatory proliferation and in the formation of hyperplastic overgrowths caused by apoptotic cells in the Drosophila wing disc. *Development* **136**, 1169-1177. doi:10.1242/dev.034017

Placzek, M. and Briscoe, J. (2018). Sonic hedgehog in vertebrate neural tube development. *Int. J. Dev. Biol.* **62**, 225-234. doi:10.1387/ijdb.170293jb

Praktiknjo, S. D., Saad, F., Maier, D., Ip, P. and Hipfner, D. R. (2018). Activation of Smoothened in the Hedgehog pathway unexpectedly increases Gαs-dependent cAMP levels in Drosophila. *J. Biol. Chem.* **293**, 13496-13508. doi:10.1074/jbc.RA118.001953

Price, M. A. and Kalderon, D. (1999). Proteolysis of cubitus interruptus in Drosophila requires phosphorylation by protein kinase A. *Development* **126**, 4331-4339.

Pusapati, G. V., Kong, J. H., Patel, B. B., Gouti, M., Sagner, A., Sircar, R., Luchetti, G., Ingham, P. W., Briscoe, J. and Rohatgi, R. (2018). G protein-coupled receptors control the sensitivity of cells to the morphogen Sonic Hedgehog. *Sci. Signal.* **11**, eaao5749. doi:10.1126/scisignal.aao5749

Qi, X., Liu, H., Thompson, B., McDonald, J., Zhang, C. and Li, X. (2019). Cryo-EM structure of oxysterol-bound human Smoothened coupled to a heterotrimeric Gi. *Nature* **571**, 279-283. doi:10.1038/s41586-019-1286-0

Raftery, L. A., Sanicola, M., Blackman, R. K. and Gelbart, W. M. (1991). The relationship of decapentaplegic and engrailed expression in Drosophila imaginal disks: do these genes mark the anterior-posterior compartment boundary? *Development* **113**, 27-33. doi:10.1093/genetics/139.2.745

Ranieri, N., Thérond, P. P. and Ruel, L. (2014). Switch of PKA substrates from Cubitus interruptus to Smoothened in the Hedgehog signalosome complex. *Nat. Commun.* **5**, 5034. doi:10.1038/ncomms6034

Rao, R., Salloum, R., Xin, M. and Lu, Q. R. (2016). The G protein Galphas acts as a tumor suppressor in sonic hedgehog signaling-driven tumorigenesis. *Cell Cycle* **15**, 1325-1330. doi:10.1080/15384101.2016.1164371

Riobo, N. A., Saucy, B., Dilizio, C. and Manning, D. R. (2006). Activation of heterotrimeric G proteins by Smoothened. *Proc. Natl. Acad. Sci. USA* **103**, 12607-12612. doi:10.1073/pnas.0600880103

Robbins, D. J., Nybakken, K. E., Kobayashi, R., Sisson, J. C., Bishop, J. M. and Thérond, P. P. (1997). Hedgehog elicits signal transduction by means of a large complex containing the kinesin-related protein costal2. *Cell* **90**, 225-234. doi:10.1016/S0092-8674(00)80331-1

Ruel, L., Gallet, A., Raisin, S., Truchi, A., Staccini-Lavenant, L., Cervantes, A. and Therond, P. P. (2007). Phosphorylation of the atypical kinesin Costal2 by the kinase Fused induces the partial disassembly of the Smoothened-Fused-Costal2-Cubitus interruptus complex in Hedgehog signalling. *Development* **134**, 3677-3689. doi:10.1242/dev.011577

Ryoo, H. D., Gorenc, T. and Steller, H. (2004). Apoptotic cells can induce compensatory cell proliferation through the JNK and the Wingless signaling pathways. *Dev. Cell* **7**, 491-501. doi:10.1016/j.devcel.2004.08.019

Schaefer, M., Petronczki, M., Dorner, D., Forte, M. and Knoblich, J. A. (2001). Heterotrimeric G proteins direct two modes of asymmetric cell division in the Drosophila nervous system. *Cell* **107**, 183-194. doi:10.1016/S0092-8674(01)00521-9

Scholz, N., Guan, C., Nieberler, M., Grotemeyer, A., Maiellaro, I., Gao, S., Beck, S., Pawlak, M., Sauer, M., Asan, E. et al. (2017). Mechano-dependent signaling by Latrophilin/CIRL quenches cAMP in proprioceptive neurons. *eLife* **6**, e28360. doi:10.7554/eLife.28360

Schwabe, T., Bainton, R. J., Fetter, R. D., Heberlein, U. and Gaul, U. (2005). GPCR signaling is required for blood-brain barrier formation in drosophila. *Cell* **123**, 133-144. doi:10.1016/j.cell.2005.08.037

Shen, F., Cheng, L., Douglas, A. E., Riobo, N. A. and Manning, D. R. (2013). Smoothened is a fully competent activator of the heterotrimeric G protein G(i). *Mol. Pharmacol.* **83**, 691-697. doi:10.1124/mol.112.082511

Singh, J., Wen, X. and Scales, S. J. (2015). The Orphan G Protein-coupled Receptor Gpr175 (Tpra40) enhances Hedgehog signaling by modulating cAMP levels. *J. Biol. Chem.* **290**, 29663-29675. doi:10.1074/jbc.M115.665810

Strigini, M. and Cohen, S. M. (1997). A Hedgehog activity gradient contributes to AP axial patterning of the Drosophila wing. *Development* **124**, 4697-4705.

Su, Y., Ospina, J. K., Zhang, J., Michelson, A. P., Schoen, A. M. and Zhu, A. J. (2011). Sequential phosphorylation of smoothened transduces graded hedgehog signalling. *Sci. Signal.* **4**, ra43. doi:10.1126/scisignal.4159ec43

Umemori, M., Takemura, M., Maeda, K., Ohba, K. and Adachi-Yamada, T. (2007). Drosophila T-box transcription factor Optomotor-blind prevents pathological folding and local overgrowth in wing epithelium through confining Hh signal. *Dev. Biol.* **308**, 68-81. doi:10.1016/j.ydbio.2007.05.007

Usui, T., Shima, Y., Shimada, Y., Hirano, S., Burgess, R. W., Schwarz, T. L., Takeichi, M. and Uemura, T. (1999). Flamingo, a seven-pass transmembrane cadherin, regulates planar cell polarity under the control of Frizzled. *Cell* **98**, 585-595. doi:10.1016/S0092-8674(00)80046-X

Wang, G., Wang, B. and Jiang, J. (1999). Protein kinase A antagonizes Hedgehog signaling by regulating both the activator and repressor forms of Cubitus interruptus. *Genes Dev.* **13**, 2828-2837. doi:10.1101/gad.13.21.2828

Wang, B., Fallon, J. F. and Beachy, P. A. (2000). Hedgehog-regulated processing of Gli3 produces an anterior/posterior repressor gradient in the developing vertebrate limb. *Cell* **100**, 423-434. doi:10.1016/S0092-8674(00)80678-9

Wettschureck, N. and Offermanns, S. (2005). Mammalian G proteins and their cell type specific functions. *Physiol. Rev.* **85**, 1159-1204. doi:10.1152/physrev.00003.2005

Wojcik, W. J. and Neff, N. H. (1984). gamma-aminobutyric acid B receptors are negatively coupled to adenylate cyclase in brain, and in the cerebellum these receptors may be associated with granule cells. *Mol. Pharmacol.* **25**, 24-28.

Yatsuzuka, A., Hori, A., Kadoya, M., Matsuo-Takasaki, M., Kondo, T. and Sasai, N. (2019). GPR17 is an essential regulator for the temporal adaptation of sonic hedgehog signalling in neural tube development. *Development* **146**, dev176784. doi:10.1242/dev.176784

Yoshiura, S., Ohta, N. and Matsuzaki, F. (2012). Tre1 GPCR signaling orients stem cell divisions in the *Drosophila* central nervous system. *Dev. Cell* **22**, 79-91. doi:10.1016/j.devcel.2011.10.027

Zhang, C., Williams, E. H., Guo, Y., Lum, L. and Beachy, P. A. (2004). Extensive phosphorylation of Smoothened in Hedgehog pathway activation. *Proc. Natl. Acad. Sci. USA* **101**, 17900-17907. doi:10.1073/pnas.0408093101

Zhao, Y., Tong, C. and Jiang, J. (2007). Hedgehog regulates smoothened activity by inducing a conformational switch. *Nature* **450**, 252-258. doi:10.1038/nature06225

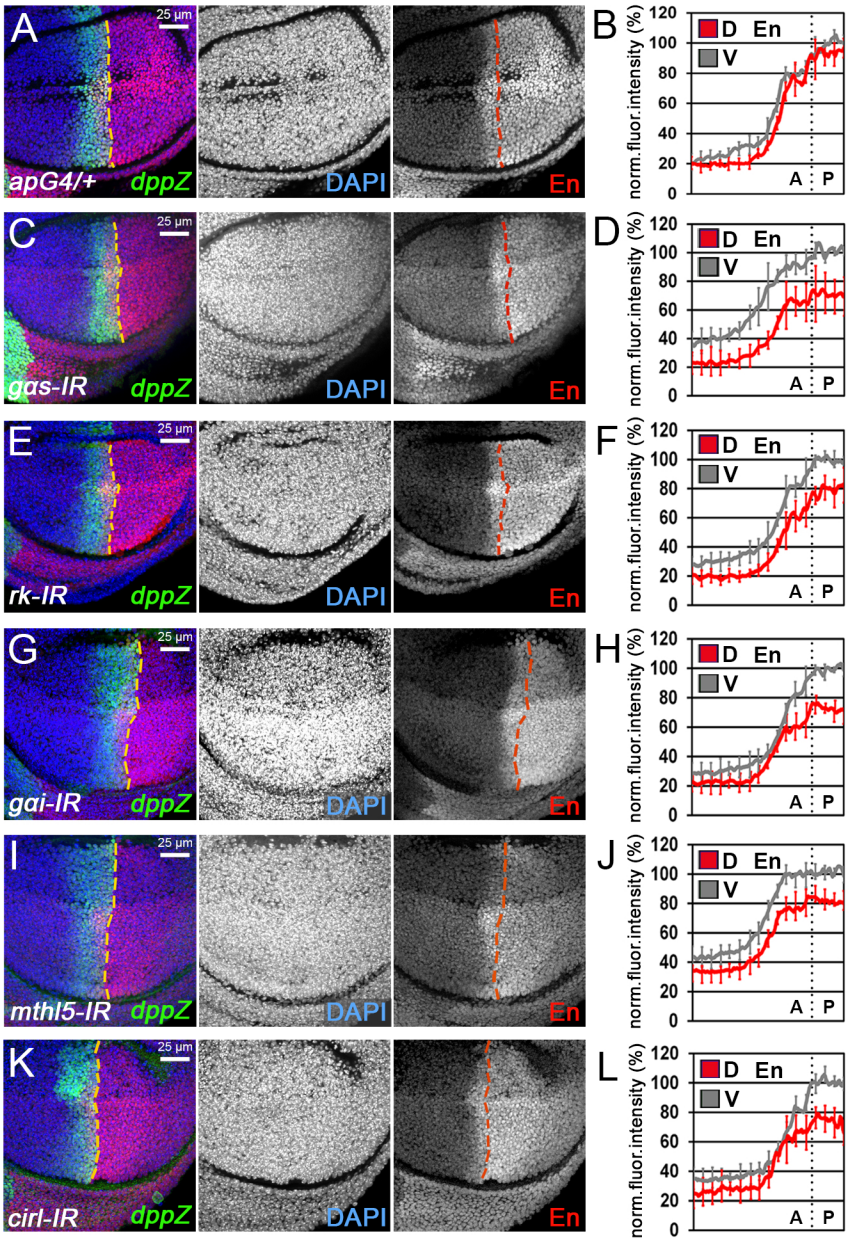

Fig. S1. Effects of GPCR depletion on anterior En in discs. (A-B) Confocal images of wing discs from control *ap-GAL4/+* animals (A) or from animals with *ap*-GAL4-driven depletion of *gαs* (C), *rk* (E), *gαi* (G), *mthl5* (I), or *cirl* (K). Discs were immunostained with antibodies against β-Gal (expressed from a *dpp* enhancer trap; *green*) and En (*red*), as well as DAPI (*blue*). Dotted lines indicate the A-P boundary. Fluorescence intensity along the A-P axis in dorsal (D) versus ventral (V) compartments is quantified in (B), (D), (F), (H), (J) and (L). In all cases, En fluorescence intensity values were normalized to the mean DAPI fluorescence value within each compartment to correct for differencese in cellularity observed in some genotypes. Graphed data represent the mean ± SD of five wing discs. Error bars are indicated every 10th data point.

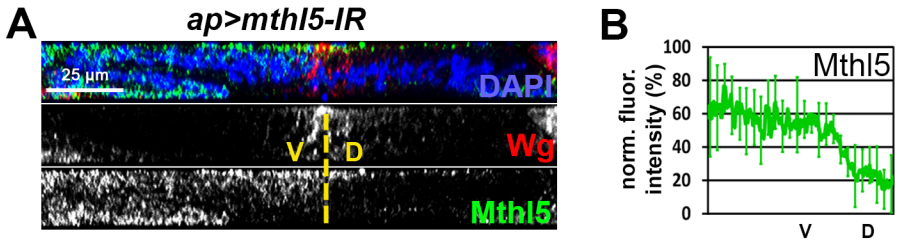

Fig. S2. Validation of anti-Mthl5 antiserum. (A) Confocal XZ section along the dorsal-ventral axis (dorsal to the right) of a wing disc expressing dsRNA targeting *mthl5* in the dorsal compartment, immunostained with antibodies against Mthl5 (*green*) and Wg (*red*) to mark the dorsal-ventral boundary (*yellow dotted line*). DAPI-stained nuclei are in *blue*. (B) Quantitation of fluorescence intensity in discs as in (A). Plot represents mean ± SD of five discs. Mthl5 staining intensity is lower in the *mthl5*-depleted dorsal compartment, confirming the specificity of the antiserum and verifying that the *mthl5* RNAi depletion in discs is efficient.

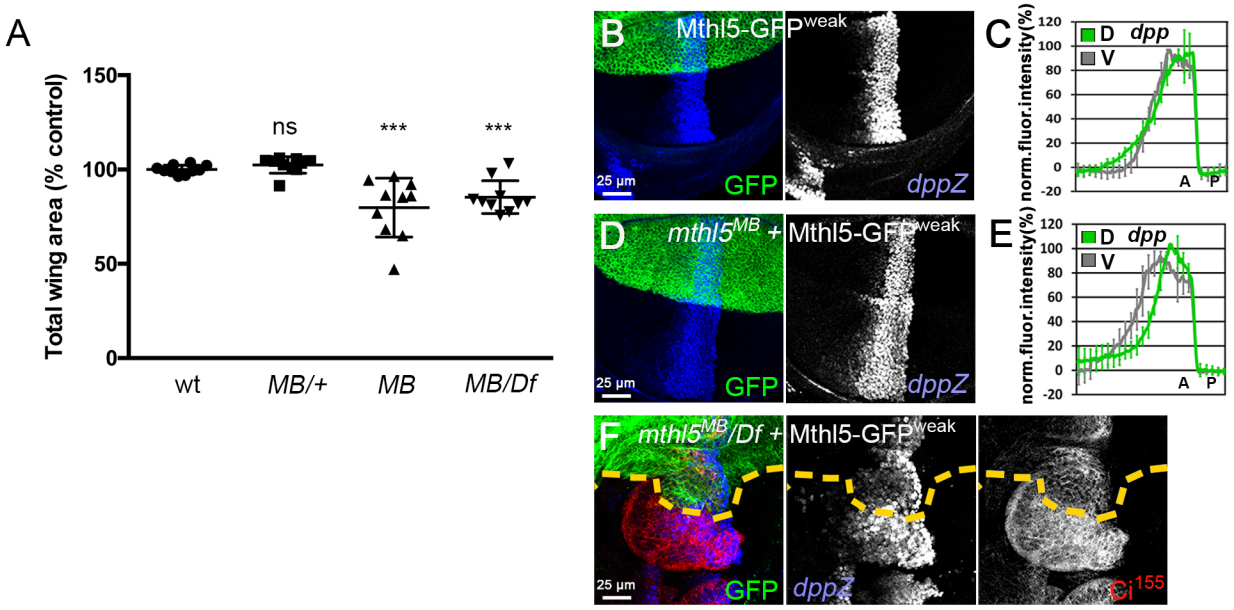

Fig. S3. Characterization of *mthl5* mutants. (A) Quantification of total wing area from wild-type, *mthl5*^{MB03076} heterozygous, *mthl5*^{MB03076} homozygous, and *mthl5*^{MB03076}*/Df(3R)BSC514* flies. *t*-test: ***, smaller than wild-type, $p<0.001$; ns, not significantly different from wild-type. *mthl5* mutant wings were smaller than normal. (B-F) Wild-type (B), *mthl5*^{MB03076} (D), or *mthl5*^{MB03076}*/Df(3R)B-SC514* (F) wing discs expressing a weaker Mthl5-GFP transgene (*green*) in the dorsal compartment under the control of *ap*-Gal4, immunostained with antibodies against β-Gal (expressed from a *dpp* enhancer trap; *blue*) and Ci^{155} (*red* in (F)).Dorsal versus ventral fluorescence intensities of discs of the genotypes in (B) and (D) are quantified in (C) and (E), respectively (mean ± SD of five discs). Mthl5-GFP expression rescued the expansion of *dpp* expression and Ci stabilization in *mthl5* mutants.

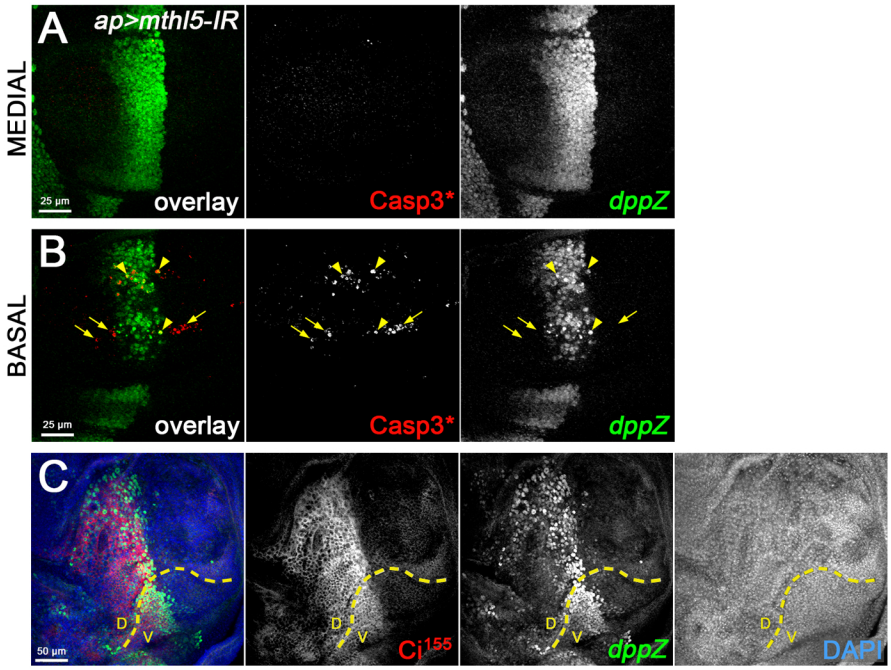

Fig. S4. Analysis of *dpp* expression and apoptosis in Mthl5-depleted wing discs. (**A-B**) Projection of confocal sections through the medial epithelial layer (**A**) and basal region (**B**) of a wing disc expressing dsRNA targeting *mthl5* in the dorsal compartment under the control of *ap*-GAL4. Disc was immunostained with antibodies against activated Caspase 3 (*red*) and β-Gal (expressed from a *dpp* enhancer trap; *green*). Arrowheads indicate pyknotic nuclei positive for both Caspase 3 and β-Gal. Arrows indicate pyknotic nuclei positive for Caspase 3 only. *dpp* was upregulated and expanded in the *mthl5*-depleted dorsal compartment even though apoptosis levels were moderate. *dpp*-expressing apoptotic cells were seen only under the *dpp* expression domain, suggesting that they represent normal *dpp*-expressing cells that have undergone apoptosis rather than cells that activated *dpp* expression as a consequence of apoptosis. (**C**) Projection of confocal sections through a $mthl5^{MB03076}/Df(3R)BSC514$ wing disc expressing P35 throughout the dorsal compartment under the control of *ap*-GAL4. Disc was stained with DAPI (*blue*) and antibodies against activated Ci^{155} (*red*) and β-Gal (expressed from a *dpp* enhancer trap; *green*). Yellow line indicates the position of the dorsal-ventral boundary. Note that this image is at half the magnification of (**A**) and (**B**). Blocking apoptosis does not prevent the dramatic expansion of the domains of Ci stabilization and *dpp* expression, which are mainly restricted to the Hhe-responsive anterior compartment. These results suggest that Hh target expansion is due to expanded Hh responsiveness rather than apoptosis.

TABLE S1. List of GPCR genes in *Drosophila* (after CD Hanlon & DJ Andrew (2015), doi: 10.1242/jcs.175158)

FBID	CG number	NAME	SYMBOL	CLASS
FBgn0025632	CG4313	-	CG4313	Rhodopsin-like/Class A
FBgn0025631	CG4322	moody	moody	Rhodopsin-like/Class A
FBgn0046687	CG3171	Trapped in endoderm 1	Tre1	Rhodopsin-like/Class A
FBgn0036742	CG7497	-	CG7497	Rhodopsin-like/Class A
FBgn0031770	CG13995	-	CG13995	Rhodopsin-like/Class A
FBgn0035331	CG8985	Myosuppressin receptor 1	MsR1	Rhodopsin-like/Class A
FBgn0264002	CG43745	Myosuppressin receptor 2	MsR2	Rhodopsin-like/Class A
FBgn0033579	CG13229	-	CG13229	Rhodopsin-like/Class A
FBgn0029768	CG16752	Sex peptide receptor	SPR	Rhodopsin-like/Class A
FBgn0053639	CG33639	-	CG33639	Rhodopsin-like/Class A
FBgn0035385	CG2114	FMRFamide Receptor	FMRFaR	Rhodopsin-like/Class A
FBgn0029723	CG6986	Proctolin receptor	Proc-R	Rhodopsin-like/Class A
FBgn0053696	CG33696	CNMamide Receptor	CNMaR	Rhodopsin-like/Class A
FBgn0034168	CG15614	-	CG15614	Rhodopsin-like/Class A
FBgn0039354	CG31096	Leucine-rich repeat-containing G protein-coupled receptor 3	Lgr3	Rhodopsin-like/Class A
FBgn0085440	CG34411	Leucine-rich repeat-containing G protein-coupled receptor 4	Lgr4	Rhodopsin-like/Class A
FBgn0003255	CG8930	rickets	rk	Rhodopsin-like/Class A
FBgn0016650	CG7665	Leucine-rich repeat-containing G protein-coupled receptor 1	Lgr1	Rhodopsin-like/Class A
FBgn0034996	CG13575	-	CG13575	Rhodopsin-like/Class A
FBgn0004622	CG7887	Tachykinin-like receptor at 99D	TkR99D	Rhodopsin-like/Class A
FBgn0004841	CG6515	Tachykinin-like receptor at 86C	TkR86C	Rhodopsin-like/Class A
FBgn0035610	CG10626	Leucokinin receptor	Lkr	Rhodopsin-like/Class A
FBgn0004842	CG5811	RYamide receptor	RYa-R	Rhodopsin-like/Class A
FBgn0259231	CG42301	Cholecystokinin-like receptor at 17D1	CCKLR-17D1	Rhodopsin-like/Class A
FBgn0030954	CG32540	Cholecystokinin-like receptor at 17D3	CCKLR-17D3	Rhodopsin-like/Class A
FBgn0038880	CG10823	SIFamide receptor	SIFaR	Rhodopsin-like/Class A
FBgn0036934	CG7395	short neuropeptide F receptor	sNPF-R	Rhodopsin-like/Class A
FBgn0037408	CG1147	Neuropeptide F receptor	NPFR	Rhodopsin-like/Class A
FBgn0038139	CG8795	Pyrokinin 2 receptor 2	PK2-R2	Rhodopsin-like/Class A
FBgn0038140	CG8784	Pyrokinin 2 receptor 1	PK2-R1	Rhodopsin-like/Class A
FBgn0038201	CG9918	Pyrokinin 1 receptor	PK1-R	Rhodopsin-like/Class A
FBgn0037100	CG14575	Capability receptor	CapaR	Rhodopsin-like/Class A
FBgn0038874	CG5911	ETHR	ETHR	Rhodopsin-like/Class A
FBgn0036789	CG13702	Allatostatin C receptor 2	AstC-R2	Rhodopsin-like/Class A
FBgn0036790	CG7285	Allatostatin C receptor 1	AstC-R1	Rhodopsin-like/Class A
FBgn0039595	CG10001	Allatostatin A receptor 2	AstA-R2	Rhodopsin-like/Class A
FBgn0266429	CG2872	Allatostatin A receptor 1	AstA-R1	Rhodopsin-like/Class A
FBgn0033058	CG14593	CCHamide-2 receptor	CCHa2-R	Rhodopsin-like/Class A
FBgn0050106	CG30106	CCHamide-1 receptor	CCHa1-R	Rhodopsin-like/Class A
FBgn0085410	CG34381	Trissin receptor	TrissinR	Rhodopsin-like/Class A
FBgn0050340	CG30340	-	CG30340	Rhodopsin-like/Class A
FBgn0002940	CG4550	neither inactivation nor afterpotential E	ninaE	Rhodopsin-like/Class A
FBgn0003248	CG16740	Rhodopsin 2	Rh2	Rhodopsin-like/Class A
FBgn0019940	CG5192	Rhodopsin 6	Rh6	Rhodopsin-like/Class A
FBgn0003249	CG10888	Rhodopsin 3	Rh3	Rhodopsin-like/Class A
FBgn0003250	CG9668	Rhodopsin 4	Rh4	Rhodopsin-like/Class A
FBgn0014019	CG5279	Rhodopsin 5	Rh5	Rhodopsin-like/Class A
FBgn0036260	CG5638	Rhodopsin 7	Rh7	Rhodopsin-like/Class A
FBgn0266137	CG18741	Dopamine 1-like receptor 2	Dop1R2	Rhodopsin-like/Class A
FBgn0024944	CG3856	Octopamine receptor in mushroom bodies	Oamb	Rhodopsin-like/Class A
FBgn0038653	CG18208	alpha2-adrenergic-like octopamine receptor	Octalpha2R	Rhodopsin-like/Class A
FBgn0011582	CG9652	Dopamine 1-like receptor 1	Dop1R1	Rhodopsin-like/Class A
FBgn0053517	CG33517	Dopamine 2-like receptor	Dop2R	Rhodopsin-like/Class A
FBgn0004573	CG12073	5-hydroxytryptamine (serotonin) receptor 7	5-HT7	Rhodopsin-like/Class A
FBgn0004514	CG7485	Octopamine-Tyramine receptor	Oct-TyrR	Rhodopsin-like/Class A
FBgn0263116	CG15113	5-hydroxytryptamine (serotonin) receptor 1B	5-HT1B	Rhodopsin-like/Class A
FBgn0004168	CG16720	5-hydroxytryptamine (serotonin) receptor 1A	5-HT1A	Rhodopsin-like/Class A
FBgn0038541	CG16766	Tyramine receptor II	TyrRII	Rhodopsin-like/Class A
FBgn0038542	CG7431	Tyramine receptor	TyrR	Rhodopsin-like/Class A
FBgn0038063	CG33976	Octopamine beta2 receptor	Octbeta2R	Rhodopsin-like/Class A
FBgn0038980	CG6919	Octopamine beta1 receptor	Octbeta1R	Rhodopsin-like/Class A
FBgn0250910	CG42244	Octopamine beta3 receptor	Octbeta3R	Rhodopsin-like/Class A
FBgn0087012	CG1056	5-hydroxytryptamine (serotonin) receptor 2A	5-HT2A	Rhodopsin-like/Class A
FBgn0261929	CG42796	5-hydroxytryptamine (serotonin) receptor 2B	5-HT2B	Rhodopsin-like/Class A
FBgn0000037	CG4356	muscarinic Acetylcholine Receptor, A-type	mAChR-A	Rhodopsin-like/Class A
FBgn0037546	CG7918	muscarinic Acetylcholine Receptor, B-type	mAChR-B	Rhodopsin-like/Class A
FBgn0035010	CG13579	-	CG13579	Rhodopsin-like/Class A
FBgn0035538	CG18314	Dopamine/Ecdysteroid receptor	DopEcR	Rhodopsin-like/Class A
FBgn0039396	CG33344	Crustacean cardioactive peptide receptor	CCAP-R	Rhodopsin-like/Class A
FBgn0025595	CG11325	Adipokinetic hormone receptor	AkhR	Rhodopsin-like/Class A
FBgn0036278	CG10698	Corazonin receptor	CrzR	Rhodopsin-like/Class A
FBgn0039747	CG9753	Adenosine receptor	AdoR	Rhodopsin-like/Class A
FBgn0029909	CG12796	muscarinic Acetylcholine Receptor, C-type	mAChR-C	Rhodopsin-like/Class A
FBgn0030437	CG4395	hector	hec	Secretin-like/Class B
FBgn0052843	CG32843	Diuretic hormone 31 Receptor	Dh31-R	Secretin-like/Class B
FBgn0033744	CG12370	Diuretic hormone 44 receptor 2	Dh44-R2	Secretin-like/Class B
FBgn0033932	CG8422	Diuretic hormone 44 receptor 1	Dh44-R1	Secretin-like/Class B
FBgn0260753	CG13758	Pigment-dispersing factor receptor	Pdfr	Secretin-like/Class B
FBgn0034219	CG6536	methuselah-like 4	mthl4	Secretin-like/Class B
FBgn0028956	CG6530	methuselah-like 3	mthl3	Secretin-like/Class B
FBgn0035623	CG17795	methuselah-like 2	mthl2	Secretin-like/Class B
FBgn0023000	CG6936	methuselah	mth	Secretin-like/Class B
FBgn0045442	CG32853	methuselah-like 12	mthl12	Secretin-like/Class B
FBgn0035847	CG7476	methuselah-like 7	mthl7	Secretin-like/Class B
FBgn0035789	CG16992	methuselah-like 6	mthl6	Secretin-like/Class B
FBgn0045443	CG31147	methuselah-like 11	mthl11	Secretin-like/Class B
FBgn0050018	CG30018	methuselah-like 13	mthl13	Secretin-like/Class B
FBgn0035132	CG17061	methuselah-like 10	mthl10	Secretin-like/Class B
FBgn0051720	CG31720	methuselah-like 15	mthl15	Secretin-like/Class B
FBgn0030766	CG4521	methuselah-like 1	mthl1	Secretin-like/Class B
FBgn0037960	CG6965	methuselah-like 5	mthl5	Secretin-like/Class B
FBgn0052476	CG32476	methuselah-like 14	mthl14	Secretin-like/Class B
FBgn0035131	CG17084	methuselah-like 9	mthl9	Secretin-like/Class B
FBgn0052475	CG32475	methuselah-like 8	mthl8	Secretin-like/Class B
FBgn0031275	CG3022	metabotropic GABA-B receptor subtype 3	GABA-B-R3	Glutamate/Class C
FBgn0260446	CG15274	metabotropic GABA-B receptor subtype 1	GABA-B-R1	Glutamate/Class C
FBgn0027575	CG6706	metabotropic GABA-B receptor subtype 2	GABA-B-R2	Glutamate/Class C
FBgn0050361	CG30361	mangetout	mtt	Glutamate/Class C
FBgn0019985	CG11144	metabotropic Glutamate Receptor	mGluR	Glutamate/Class C
FBgn0001085	CG17697	frizzled	fz	Frizzled/Class F
FBgn0016797	CG9739	frizzled 2	fz2	Frizzled/Class F
FBgn0027343	CG16785	frizzled 3	fz3	Frizzled/Class F
FBgn0027342	CG4626	frizzled 4	fz4	Frizzled/Class F
FBgn0003444	CG11561	smoothened	smo	Frizzled/Class F
FBgn0033313	CG8639	Calcium-independent receptor for alpha-latrotoxin	Cirl	Frizzled/Class F
FBgn0024836	CG11895	starry night	stan	Frizzled/Class F
FBgn0039818	CG11318	-	CG11318	Frizzled/Class F
FBgn0039821	CG15556	-	CG15556	Frizzled/Class F
FBgn0051660	CG31660	smog	smog	-
FBgn0051760	CG31760	-	CG31760	-
FBgn0265002	CG44153	-	CG44153	-
FBgn0039419	CG12290	-	CG12290	-
FBgn0052447	CG32447	-	CG32447	-
FBgn0030466	CG15744	-	CG15744	-
FBgn0052547	CG32547	-	CG32547	-
FBgn0000206	CG8285	bride of sevenless	boss	-

Table S2: Summary of GPCR RNAi transgenic strains and phenotypes

GPCR	RNAi Strain	RNAi Depletion Phenotype
Trapped in endoderm 1	V108952	lethal
	V7220	WT
	TRiP.HMS00433	WT
	TRiP.JF02751	WT
	TRiP.HMS00599	WT
CCK-like receptor at 17D3	V102039	WT
	V1815	lethal, few wingless escapers
	V9154	WT
Moody	V1800	WT
Tachykinin-like receptor at 86C	V13392	WT
	V107090	WT
Rickets	V905	weak inflation defects, small wings, decreased Hh signaling
	V105360	weak inflation defects, small wings, decreased Hh signaling
CG4313	V107434	WT
Starry night	V107993	weak inflation defects, small wings, decreased Hh signaling
	V1665	WT
	V51379	WT
	V51382	WT
Diuretic hormone 31 receptor 1	V101995	WT
	V8777	WT
Cirl	V100749	increased Hh signaling
	V29969	lethal
	TRiP.JF02674	WT
	TRiP.HMS00136	WT
Methuselah	V102303	increased Hh signaling
	V330139	WT
	TRiP.HMS05784	WT
	TRiP.JF02645	WT
Methuselah-like 1	V33136	crumpled and fluid-filled wings
	V107488	WT
Methuselah-like 2	V26815	WT
	V330202	WT
Methuselah-like 3	V104033	WT
	V49623	WT
	V49624	WT
Methuselah-like 4	V50752	weak inflation defects, small wings, decreased Hh signaling
	TRiP.HMC02422	WT
Methuselah-like 5	V101593	increased Hh signaling
	V3390	WT
	TRiP.HMC06002	WT
Methuselah-like 6	V108048	strong inflation defects
	V47948	WT
	V47949	WT
Methuselah-like 8	V100246	strong inflation defects, decreased Hh signaling
	V4071	WT
	TRiP.HMJ22590	WT
Methuselah-like 9	V108967	strong inflation defects, decreased Hh signaling
	V2769	WT
	V2770	WT
	TRiP.HMC03141	WT
	TRiP.HMJ24136	WT
Methuselah-like 10	V100829	WT
	V51425	WT
CG15744	V4801	weak inflation defects, small wings, decreased Hh signaling
	V28516	WT
	V42497	WT
Metabotropic GABA-B receptor subtype 2	V1785	increased Hh signaling
	TRiP.JFO2779	increased Hh signaling
	V110268	increased Hh signaling
	TRiP.HMC02975	WT
CG32447	V102740	lethal, few wingless escapers
	V5417	WT
	TRiP.HMJ22835	WT